

**ANALYSIS OF TIME SYNCHRONIZATION ERRORS IN HIGH DATA
RATE UWB-OFDM DATA LINKS**

by

LAKESHA D. BATES
B.S. Bethune-Cookman College, 2001

A thesis submitted in partial fulfillment of the requirements
for the degree of Master of Science
in the Department of Electrical and Computer Engineering
in the College of Engineering and Computer Science
at the University of Central Florida
Orlando, Florida

Fall Term
2004

© 2004 Lakesha Bates

ABSTRACT

Emerging Ultra Wideband (UWB) Orthogonal Frequency Division Multiplexing (OFDM) systems hold the promise of delivering wireless data at high speeds, exceeding hundreds of megabits per second over typical distances of 10 meters or less. The purpose of this Thesis is to estimate the timing accuracies required with such systems in order to achieve Bit Error Rates (BER) of the order of magnitude of 10^{-12} and thereby avoid overloading the correction of irreducible errors due to misaligned timing errors to a small absolute number of bits in error in real-time relative to a data rate of hundreds of megabits per second.

Our research approach involves managing bit error rates through identifying maximum timing synchronization errors. Thus, it became our research goal to determine the timing accuracies required to avoid operation of communication systems within the asymptotic region of BER flaring at low BERs in the resultant BER curves. We propose pushing physical layer bit error rates to below 10^{-12} before using forward error correction (FEC) codes. This way, the maximum reserve is maintained for the FEC hardware to correct for burst as well as recurring bit errors due to corrupt bits caused by other than timing synchronization errors.

To Dr. Harriett G. Jenkins. Thank you for giving the NASA Harriett G. Jenkins Pre-Doctorial Fellowship Program your positive energy and warm spirit. As one of the fellowship recipients, I swore into the fellowship program to honor your name with pride through achievement in the engineering field, and I have kept my promise. This thesis is one of my many approaching achievements dedicated to you. I very much appreciate you. Your legacy will live with me forever!

ACKNOWLEDGMENTS

At the beginning of my Master's of Science education I started out in the satellite communications area. Later through the guidance of my Academic Advisor: Dr. W. Linwood Jones, Kennedy Space Center Personnel: Richard Nelson, Dr. Gary Bastin, and Erik Denson, I was encouraged to conduct research in the area of Ultra Wideband, which was the best change of my academic career.

My advisor, Dr. W. Linwood Jones (Dr. J) drove in his personal vehicle, on his own time, to meet with personnel at Kennedy Space Center (KSC) to discuss research possibilities. He also helped polish my research proposal which was ultimately chosen as one of the top twenty research proposals in the United States for the Harriett Jenkins Pre-doctoral Fellowship Award. I received this level of support from Dr. J throughout my entire graduate career and I sincerely thank him for all of his efforts.

Richard Nelson, Range Systems and Design Development Branch Chief, (KSC) made it possible for me to tie in my research topic to a NASA mission and write the proposal for the Harriett Jenkins Pre-Doctoral Fellowship Award. This prestigious Fellowship award is only awarded to the top twenty applicants in the United States per year and I was able to receive it thanks to him.

Dr. Gary Bastin (KSC) is the genius who I spent most of my time with conducting research at KSC. It was through him that I was able to learn, grow, and develop an understanding of Ultra Wideband. To say the least, my research thesis would not have been possible without his guidance and support. I can not thank him enough for all the time he spent

helping me between his work schedule, checking my research results, giving me expert advise on the subject matter, helping me to develop and define the theoretical and experimental analysis, and helping me polish my thesis document- you name it, and he did it in helping me complete my research. I graciously thank him for all of his energy and patience. I truly learned a lot through his guidance. Also, Gary introduced me, through a phone conference, to Mr. Kevin Davis of Time Domain Corporation, Huntsville, AL. I thank Mr. Davis for his support of this thesis through expediting the out-of-warranty repair of Time Domain's PulsON 200 Evaluation Kit to complete and conduct the PulsON 200 Test Cases contained in this thesis.

Erik Denson, Range Communication Lead, was my mentor while at KSC. He made sure I had access to all the tools and software that I needed to support this thesis. He also provided mentor guidance that helped me to get through some of the tough days and I thank him.

Special thanks go out to all of my academic supporters: Thesis Committee Members, Kennedy Space Center, Goddard Flight Space Center, NASA Harriett Jenkins Pre-Doctorial Fellowship Program, UNCFSP (United Negro College Fund Special Programs), Intel Corporations, National Consortium for Graduate Degrees for Minorities in Engineering and Science, Inc. (GEM), Time Domain Corporation, Northrop-Grumman (Integrated Systems), University of Central Florida, and Friends and Family- especially my Grandma, Betty Bates for the home-made food and Ronald Valykeo for keeping me laughing, wondering what kind of work I was doing that could keep me up night and day for months. (My Thesis)

TABLE OF CONTENTS

LIST OF FIGURES	ix
LIST OF TABLES	xi
LIST OF ABBREVIATIONS	xii
CHAPTER 1 INTRODUCTION	1
1.1 UWB Overview	1
1.1.1 UWB Concepts	4
1.2 OFDM Overview	6
1.3 Thesis Organization	8
CHAPTER 2 TIMING JITTER IN UWB-OFDM COMMUNICATION SYSTEMS.....	9
2.1 OFDM Technique	9
2.2 Timing Error Effects on System Performance.....	12
2.3 Timing Jitter and Phase Noise relationship	12
2.4 Tikhonov Approximation of Timing Error	14
CHAPTER 3 BIT SYNCHRONIZATION.....	16
3.1 Analytical Solutions for BER Performance	17
3.1.1 Conditional Error Probabilities	18
3.1.1.1 Manchester Coded Data	19
3.1.1.2 NRZ Coded Data.....	19
3.1.1.3 RZ Coded Data	20
3.1.1.4 Miller Coded Data.....	20
3.1.2 Establishing Average Error Probability at the Receiver	21
3.2 Test Case with PulsON 200 Radios	24
3.2.1 Test Procedures	26
CHAPTER 4 FINDINGS.....	31
4.1 Results Overview	31
4.2 BER Effects Due to Timing Errors.....	31
4.3 PulsON 200 Test Case	38

4.3.1 Required Equipment and Test Setup.....	39
4.3.2 Test Case Results	40
4.4 Assessment of Timing Uncertainties	43
4.5 Analysis of Effects on UWB-OFDM System with High Data Rates	46
CHAPTER 5 CONCLUSION.....	48
5.1 Summary of Results.....	48
5.2 Recommendations for Future Work.....	49
APPENDIX A PERFORMANCE ANALYSIS TOOL	50
APPENDIX B DIGITAL SIGNALING FORMATS	63
APPENDIX C RELATIONSHIP BETWEEN E_b/N_0 AND S/N	66
APPENDIX D Q-FUNCTION, ERF, AND ERFC	70
REFERENCES	73

LIST OF FIGURES

Figure 1: Emitted Signal Power vs. Frequency in Giga Hertz.....	3
Figure 2: UWB vs. 802.11a Potential Throughput Data Rates at distances in Meters (Picture from Ultra-Wideband/ a Disruptive RF Technology [11]).....	4
Figure 3: Gaussian monocycle pulse and ideal received monocycle pulse (Picture from Hailiang Mei Masters thesis [14])	5
Figure 4: De-multiplexed High Data Rate OFDM Data Stream.....	6
Figure 5: Overlapping orthogonal sub-carriers in OFDM symbol	7
Figure 6: OFDM Symbol.....	10
Figure 7: OFDM Block Diagram.....	14
Figure 8: Performance Analysis Tool’s graphical user interface for PulsON 200 Receiver.....	27
Figure 9: Theoretical BER vs. Eb/No for PulsON 200 Flip Modulation.....	29
Figure 10: Representation of timing errors in a digital signal	32
Figure 11: Representation of Distortions in a Digital Signal.....	33
Figure 12: Probability of error for Manchester coded data conditioned on UI timing errors.....	34
Figure 13: Probability of error for RZ coded data conditioned on UI timing errors	35
Figure 14: Probability of error for Miller coded data conditioned on UI timing errors	36
Figure 15: Probability of error for NRZ coded data conditioned on UI timing errors	37
Figure 16: Flip Modulation (Picture from K.K Lee UWB presentation of Flip-Modulation).....	39
Figure 17: PulsON 200 Evaluation Kit Setup (Picture from [6])	40
Figure 18: Flip Modulation Theoretical Curve vs. PulsON 200 Data Collected at 9.6 Mbps.....	43
Figure 19: Manchester’s Average Probability of Error Curves with extrapolated PulsON 200 Data.....	45
Figure 20: PAT Statistics Frame Area.....	51

Figure 21: PAT Test Case @ 330 feet distance	55
Figure 22: PAT Test Case @ 330 feet distance	55
Figure 23: PAT Test Case @ 345 feet distance	56
Figure 24: PAT Test Case @ 300 feet distance and VGA 31.....	56
Figure 25: PAT Test Case @ 16.40 feet or 5 meters distance	57
Figure 26: PAT Test Case @ 300 feet distance	57
Figure 27: PAT Test Case @ 300 feet distance	58
Figure 28: PAT Test Case @ 200 feet distance	58
Figure 29: PAT Test Case @ 200 feet distance	59
Figure 30: PAT Test Case @ 100 feet distance	59
Figure 31: PAT Test Case @ 10 feet distance	60
Figure 32: PAT Test Case @ 5 feet distance	60
Figure 33: PAT Test Case @ 26.24 feet or 8 meter distance	61
Figure 34: PAT Test Case @ 26.24 feet or 8 meter distance	61
Figure 35: PAT Test Case @ 26.24 feet or 8 meter distance	62
Figure 36: PAT Test Case @ 26.24 feet or 8 meter distance	62
Figure 37: Binary Line Coding.....	64

LIST OF TABLES

Table 1: Analytical Equation Definitions 23

Table 2: PulsON 200 Collection of Data Rate vs. Range Test Cases..... 42

LIST OF ACRONYMS

Bit Error Rates	BER
Binary Phase Shift Keying	BPSK
Bandwidth	BW
Clock and data recovery	CDR
Energy per bit	EB
Federal Communications Commission	FCC
Forward error correction	FEC
Hertz	Hz
Inverse Fast Fourier Transform	IFFT
Multi-Band OFDM Alliance	MBOA
Mega Bits per second	Mbps
Multiplexer	MUX
Effective noise	NEFF
Orthogonal Frequency Division Multiplexing	OFDM
On/Off Keying	OOK
Pulse Amplitude Modulation	PAM
Performance Analysis Tool	PAT
Probability density function	PDF
Physical	PHY
Pulse Position Modulation	PPM

Radio frequency	RF
Unit Interval	UI
Ultra Wideband	UWB
Wireless personal area networking	WPAN

CHAPTER 1

INTRODUCTION

In the near future, wireless broadband communications systems will require data rates exceeding hundreds of mega bits per second (Mbps). To address these approaching demands, emerging Ultra Wideband (UWB) Orthogonal Frequency Division Multiplexing (OFDM) offers an ideal physical (PHY) layer solution to address wireless personal area networking (WPAN) needs over short ranges. As UWB modulation becomes better understood and data rates increase to near their high data rate potentials, the control of timing synchronization errors will become ever more critical in measuring UWB's system performance parameters. This thesis explores the timing accuracies required to support the operation of UWB OFDM systems in such a future communication landscape.

1.1 UWB Overview

UWB is a term used to represent a system or signal that has a very large bandwidth. Federal Communications Commission (FCC) originally defined UWB devices as any device having a fractional bandwidth of greater than 0.25 or occupying 1.5 GHz or more of spectrum. Recent revisions for those two values were modified to 0.20 and 500MHz, respectively [10]. UWB signals' fractional bandwidth (BW) is defined by:

$$\eta = 2 \cdot \frac{(f_H - f_L)}{(f_H + f_L)} \tag{1-1}$$

where

η = Fractional_Bandwidth

f_H = Upper Frequency of -10dB Emmission Point

f_L = Lower Frequency of -10dB Emmission Point

The center frequency is defined as the average of the upper and lower frequency points, i.e.

$$f_c = \frac{f_H + f_L}{2} \quad (1-2)$$

With such large defined bandwidths, UWB communications hold the promising ability to provide high data rates, at low cost, with very low power consumption. Because of this allure, UWB has become extremely popular as a possible modulation method for a wide range of short-range applications. February 14, 2002, marked the start of the era where unlicensed usage of this newly defined wireless technology was approved by the FCC for commercial use. When the FCC ruled that UWB radio transmission could legally operate over the range from 3.1 GHz up to 10.6 GHz, at a limited transmit power of -41 dBm/MHz, engineers and scientists began development of new networking devices for short-range, wireless applications that could take advantage of the possibilities inherent with UWB modulation. The reason was simple, because with the availability of such a wide swath of spectrum, a higher channel capacity could be achieved than with currently used conventional radios (i.e. 802.11a/b/g). According to Shannon's Theorem:

$$C = B \log_2 \left(1 + \frac{S}{N} \right) \quad (1-3)$$

where C is the channel capacity (in bits/sec), B is the channel bandwidth in Hertz (Hz) and S/N is the signal to noise power ratio at the input to the digital receiver [6]. This equation shows two ways to increase channel capacity C in a digital system; either by increasing bandwidth B and/or by increasing signal to noise ratio S/N. However, since channel capacity grows linear with bandwidth and only approximately logarithmically to the base-2 power with signal to noise ratio, a wider bandwidth system has an inherent advantage versus a narrower bandwidth system in achieving a higher channel capacity for a given percentage increase. For example, when comparing UWB spectrum to the 802.11a spectrum in Figure 1, we see that 802.11 has high emitted signal power with a narrow bandwidth. Conversely, UWB has low emitted signal power spectral density with wide bandwidth.

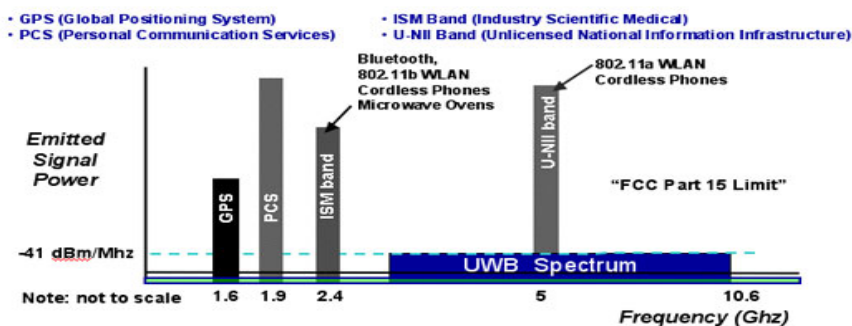


Figure 1: Emitted Signal Power vs. Frequency in Giga Hertz

Figure 2 shows that, through Shannon's Theorem, UWB's throughput data rates are significantly higher at distances of 10 meters or less than the currently used 802.11 standard.

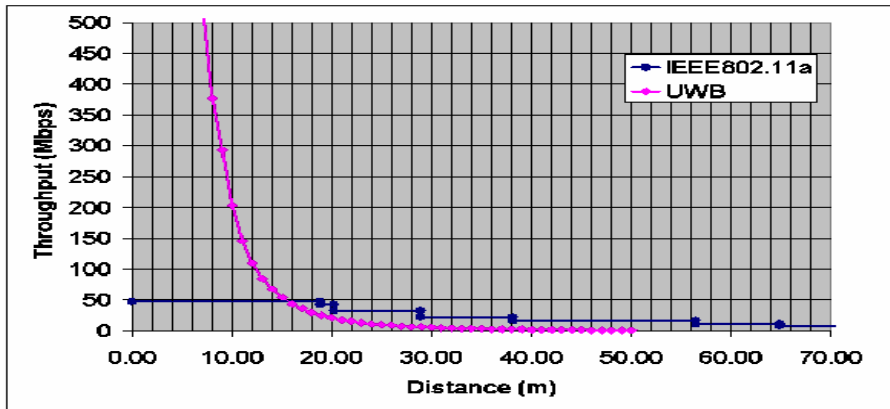


Figure 2: UWB vs. 802.11a Potential Throughput Data Rates at distances in Meters (Picture from Ultra-Wideband/ a Disruptive RF Technology [11])

1.1.1 UWB Concepts

Most radio technologies in use today employ sinusoidal carriers for radio transmissions. On the other hand, Ultra Wideband (UWB) technologies communicate at base-band without the use of a carrier. Formally referred to as “Impulse Radio,” or “Carrier-less Radio,” UWB radios communicate using short, base-band pulses, typically of duration on the order of a nanosecond. When these pulses are applied to an appropriately designed antenna, the pulses propagate over physical distances with distortions. The antennas behave as filters, and even in free space, a differentiation of the pulse waveform occurs as the wave radiates [10].

The basic waveform of a UWB signal is an approximation of a Gaussian pulse, known as a Gaussian monocycle pulse. These Gaussian monocycle pulses are usually transmitted using

Pulse Position Modulation (PPM) pulses, however, due to distortions by antennas and the channel, the received pulse differs in the time-domain from its original transmitter output pulse shape. An ideal pulse shape propagating in free space can be modeled as the first derivative of the Gaussian monocycle. The response of the received antenna to free-space propagating pulse can be approximated by the second derivative of the transmitted pulse. For example, when the pulse generated by the transmitter is Gaussian, Ramirez-Mireles and Scholtz show that an idealized received pulse can be modeled as [12]:

$$W_{\text{rec}}(t) = \left[1 - 4 \pi \left(\frac{t - t_d}{\tau_n} \right)^2 \right] \exp \left[-2 \pi \left(\frac{t - t_d}{\tau_n} \right)^2 \right] \quad (1-4)$$

where (W_{rec}) represents the received waveform, (t_d) represents the location of the pulse center and (τ_n) represents a parameter that determines the temporal width of the pulse. In Figure 3, we show the transmitted Gaussian monocycle pulse and the ideal received monocycle pulse at the antenna output.

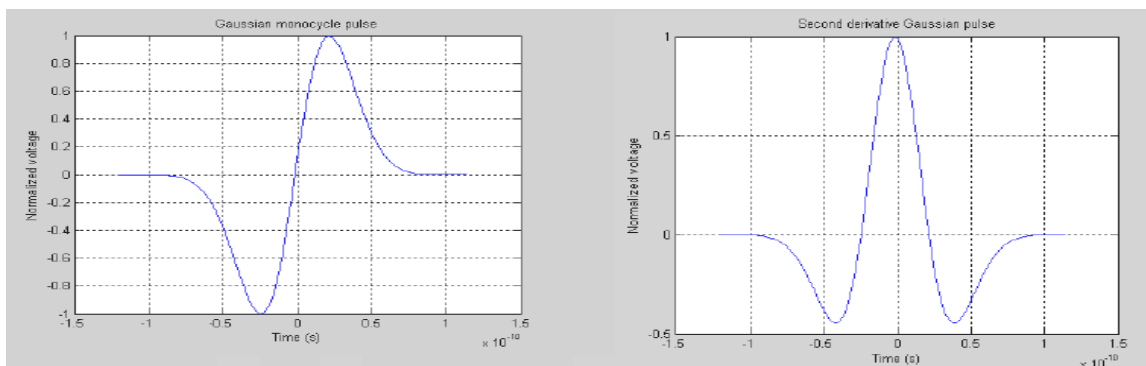


Figure 3: Gaussian monocycle pulse and ideal received monocycle pulse (Picture from Hailiang Mei Masters thesis [14])

1.2 OFDM Overview

Instead of using the traditional PPM, Pulse Amplitude Modulation (PAM), Binary Phase Shift Keying (BPSK), and On/Off Keying (OOK) modulations, an alternate approach for modulating UWB Pulses is achieved through OFDM. OFDM is a modulation technique suitable for high data rate systems. One prominent emerging UWB system developed by the Multi-Band OFDM Alliance (MBOA: www.multibandofdm.org) uses the modulation technique (OFDM) to occupy the statutory wide bandwidths permitted for UWB systems. The basic idea of the classical OFDM involves splitting a high-rate data stream X_N into a number of lower rate streams that are transmitted simultaneously at different frequencies over a number of sub-carriers (X_0, X_1, \dots, X_{N-1}) (See Figure 4). Since UWB-OFDM is generally a carrier-less technique, than it uses sub-bands instead of sub-carriers.

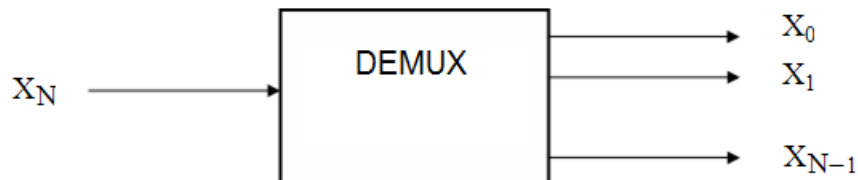


Figure 4: De-multiplexed High Data Rate OFDM Data Stream

In UWB-OFDM the sub-band pulse used for transmission is a rectangular pulse. With this rectangular pulse the task of pulse forming and modulation can be simply implemented with an Inverse Fast Fourier Transform (IFFT) of the sub-bands. At the receiver, according to the

Fourier Transform Theorem, the rectangular pulse shaped sub-banded pulses in UWB-OFDM will lead to the $[\sin(x)/x]$ spectrum. When the signal is Muxed back together, it will look like Figure 5. To obtain high spectral efficiency, the frequency response of the sub-banded channels are overlapped and orthogonal, which means that where the signal is evaluated (at the maximum peak), the value of all other signals are zero.

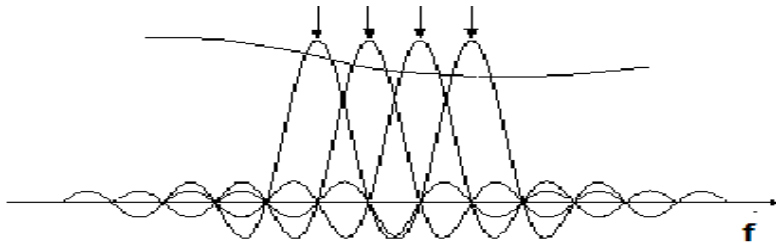


Figure 5: Overlapping orthogonal sub-carriers in OFDM symbol

Major benefits of the OFDM technique include higher spectral efficiency, resiliency to radio frequency (RF) interference, and lower multi-path distortion [4]. On the other hand, OFDM shortcomings evolve through its high sensitivity to frequency and time synchronization error compared to single carrier system [4]. Frequency synchronization error results from misalignment in sub-band frequencies due to fluctuations in radio frequency oscillators or channel's Doppler frequency introducing inter carrier interference (ICI). Timing synchronization errors refer to the incorrect timing of the OFDM symbols at the demodulator introducing inter symbol interference (ISI) [3]. Both ICI and ISI cause bit errors in a UWB-OFDM system. The focus of this thesis is to analyze how accurate timing synchronization errors must be to obtain a bit error rate of 10^{-12} , or better, assuming perfect frequency synchronization.

We will take a closer examination of this phenomenon in Chapter 2.

Although currently there are two major UWB proposals, consisting of single band and multi-band impulse-centered approaches, both with their own advocates fighting for their approach to become the accepted IEEE and FCC standard, in this thesis we focus on the multi-banded OFDM approach and its concepts and limitations. This focus is chosen since the multi-band approach currently has achieved more favor among the candidate approach to become the universal UWB standard.

1.3 Thesis Organization

The importance of controlling timing synchronization errors was established earlier in this chapter. Next, we follow this chapter with discussions regarding timing synchronization errors in UWB-OFDM systems. Then, in Chapter 3, we present our methodologies for analytical solutions for bit synchronization effects on BER (Bit Error Rate). Chapter 4 displays our results from analytical and experimental analyses and concludes with a hypothesis of the timing error effects. Finally, in Chapter 5 we conclude the thesis by restating our thesis objectives, documenting why timing synchronization is important, and summarizing the effect on BER performance if the timing accuracies are not maintained in an UWB-OFDM data link. In addition, we give recommendations for future research, for expanding on the results of this thesis.

CHAPTER 2

TIMING JITTER IN UWB-OFDM COMMUNICATION SYSTEMS

Measured performance of a digital data transmission system usually is obtained through analyzing the probability of error at a given bit error rate and signal-to-noise ratio. As the UWB systems evolve into their expected achievable high data rate values, controlling timing synchronization errors becomes essential since timing errors cause bit errors that degrade system performance. To present the concept of “How timing errors affect UWB-OFDM system performance”, this chapter is divided into three parts. First we describe the OFDM symbol structure. Then, we express how timing errors in the OFDM symbols affect the system’s performance and third we analyze the impact of timing jitter in digital communication systems. This chapter concludes with a Tikhonov approximation for estimating the timing error.

2.1 OFDM Technique

OFDM is a flexible technique that increases bandwidth efficiency, resiliency to radio frequency (RF) interference, and lower multi-path distortion. For example, if interference with an existing narrowband system occurs, UWB-OFDM permits simply by not using one or more particular sub-bands. This technique can be thought of as analogous to a combination of multi-carrier modulation (MCM) and frequency shift keying (FSK). MCM divides a data stream into several bit streams and modulates each bit stream onto sub-carriers [16]. FSK transmits data onto one carrier from multiple orthogonal carriers. Orthogonality between the sub-bands among an UWB-OFDM modulation format is accomplished by separating the bands by an integer multiple

of the inverse of symbol duration of the parallel bit streams [4]. Orthogonality in the symbol is crucial because it helps to eliminate inter-symbol interference (ISI) and inter-carrier interference (ICI). This is best done by adding a guard time insertion or a cyclic prefix (CP) to the beginning of the OFDM symbol. CP involves attaching a copy of the last part of the OFDM symbol to the beginning of the symbol as shown in Figure 6.

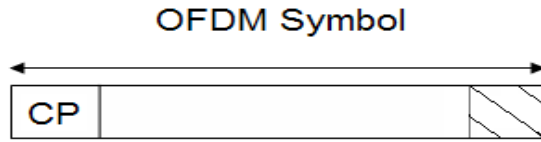


Figure 6: OFDM Symbol

In the transmitter, after the parallel data of N sub-channels are modulated onto N sub-carriers (d_0, d_1, \dots, d_{N-1}), where each d_N represents a complex number, they are fed into an Inverse Fast Fourier Transform (IFFT). The transmitted data is given by [5]:

$$s(t) := \sum_{k=-\infty}^{\infty} \sum_{i=0}^{N-1} d_i(k) \exp[j2\pi f_i(t - kT_s)] f(t - kT_s) \quad (2-1)$$

where T_s is the symbol duration of the OFDM pulse and f_i ($i=0,1,\dots,N-1$) is the frequency of the i th sub-carrier given by [5]:

$$f_i := f_0 + \frac{i}{T_s} \quad (2-2)$$

Here, $f(t)$ is the pulse waveform of each of the symbols and it is defined as

$$f(t) = \begin{cases} 1, & (0 \leq t \leq T_s) \\ 0 & (\text{otherwise}) \end{cases} \quad (2-3)$$

After the IFFT process, the signal $s(t)$ goes through a guard time insertion circuit where the cyclic period is added so inter-symbol interference can be avoided as much as possible.

One requirement of adding a CP to the symbol is that it should be longer than the impulse response of the channel. When the CP to the symbol is longer than the impulse response of the channel, it acts as a guard space between the sub-carriers. The guard time is chosen larger than the expected delay spread, such that multi-path components from one symbol cannot interfere with the next symbol [15]. This eliminates ISI and ICI almost completely. However, some residual ICI may still exist. This happens when the multi-path delay becomes larger than the guard time. At this point, the system may manifest timing errors due to the cumulative effects of multi-path delay variations.

At the output of the guard time insertion circuit, the OFDM symbol is given by:

$$\frac{d}{dt} s(t) := \sum_{k=-\infty}^{\infty} \sum_{i=0}^{N-1} d_i(k) \exp[j2\pi f_i(t - kT_{\text{total}})] \frac{d}{dt} f(t - kT_{\text{total}}) \quad [5] \quad (2-4)$$

where the modified pulse waveform of each symbol is defined as

$$\frac{d}{dt}f(t) = \begin{cases} 1 & (-T_g \leq t \leq T_s) \\ 0 & (t < -T_g, t > T_s) \end{cases} \quad [5] \quad (2-5)$$

2.2 Timing Error Effects on System Performance

Timing signals play several of different roles in communication systems. One example evolves in digital systems, where clock signals are used to transfer logic signals in and out of registers at times when their values are valid. The maximum clock frequency is usually limited by the propagation delay of the logic circuits between registers. In high bandwidth digital input/output systems, however, the data transfer rate can be limited by uncertainty in the clocks used to transfer the data [21]. Fixed offsets between transmit and receive clocks or timing errors due to noise comprise this uncertainty.

Timing errors in UWB-OFDM are simply a short variation of the OFDM sub-band's bit timing from its ideal time slot location. A bit's timing is simply the composite effect of multiple monocycles acting in concert due to various multi-path delays acting in addition to the composite effect of digital circuitry timing errors. Effects of errors in the time base of the signal, due to timing errors can also limit performance parameters such as achievable bit rates of the system. When this happens the system is said to have a degraded performance due to timing errors.

2.3 Timing Jitter and Phase Noise relationship

Oscillator or clock uncertainties in synchronous digital systems can degrade a system's

performance, resulting from in bit errors. Phase noise and timing jitter result from uncertainties in the clock's oscillator output. Phase noise defines the frequency output of the oscillator. For example, when the output to a noisy phase oscillator is given by:

$$V(t) = V_o \cdot \cos[\omega_o(t) + \phi(t)] \quad [17] \quad (2-6)$$

then

$$\phi(t) \quad (2-7)$$

is the phase noise also referred to as the spectral density of phase fluctuation. The random fluctuations of phase that are responsible for phase noise, can also be observed in the time domain as timing jitter. Given that timing jitter is a measure of variation in the time domain, it ultimately describes how far a bit period wanders from its ideal location. In OFDM systems, controlling timing jitter in the sub-carriers calls for precise synchronization at the OFDM demodulator. This control involves determination of the starting sample of the *i*th OFDM symbol such that the CP can be disregarded and the OFDM symbol can be properly realigned [3]. For example, consider the OFDM block diagram shown in Figure 7. Before the OFDM symbol can be multiplexed back together and the orthogonality of the symbol at the receiver is preserved, timing errors must be controlled or even corrected to some degree. Otherwise, the system will experience inter-carrier interference (ICI). ICI is crosstalk between different sub-carriers, which means that the sub-carriers are no longer orthogonal in signal space [15]. The orthogonality of the sub-carriers can be maintained and individual sub-carriers can be separated by using an FFT

(Fast Fourier Transform) circuit when there is no inter-symbol interference (ISI) and inter-carrier interference introduced by transmission channel distortion [1]. In reality, these conditions cannot be obtained. To manage distortion caused by the transmission channel, in the next chapter we introduce a method for estimating the timing accuracy required for achieving a given BER performance for a high data rate UWB-OFDM digital link.

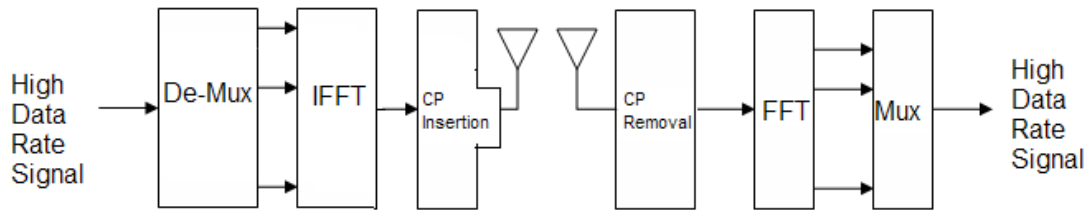


Figure 7: OFDM Block Diagram

2.4 Tikhonov Approximation of Timing Error

In OFDM bit symbols there will always be some fluctuation in the bit symbol's ideal timing. This fluctuation can be estimated around the ideal timing's mean value. Since the timing errors are random values, to estimate fluctuation in timing we characterize the actual timing using probability density function (PDF). The PDF shows how the actual bit timing estimate can be before or after the ideal value.

In literature [3, 18, 19, 20] we find that timing errors are usually characterized with a Gaussian or a Tikhonov pdf. However, we used the Tikhonov pdf so that we can obtain a more representative characterization of the bit synchronizer statistical properties in agreement with

observed properties. Chapter 3 displays the use of the Tikhonov approximation of timing errors.

CHAPTER 3

BIT SYNCHRONIZATION

This chapter introduces and presents methods and procedures for estimating the timing accuracy required for achieving a given BER performance for a high data rate UWB-OFDM digital link. Through our analysis we develop equations to determine and identify maximum timing synchronization errors of high data rate links incorporating Manchester (Bi-Phase), Miller, RZ, or NRZ coded data.

Most high-speed communication systems have a low tolerance for bit errors; the allowable uncorrected BER for such systems operating in the hundreds of Mbps typically must fall between 10^{-9} and 10^{-12} to prevent introducing error correction overload within the error correction hardware. This means that the BER impacts of synchronization and timing errors must be analyzed to estimate the timing accuracies required to avoid overloading the correction of irreducible errors due to misaligned timing errors.

In previous studies [3, 18], timing error analyses have been investigated performance in bit error regions ranging from 10^{-3} to 10^{-6} . Such a lower-performance BER is entirely appropriate for low speed communication systems operating at data rates only in the tens of Mbps. Unfortunately, these previously investigated regions are not sufficient for proposed high speed UWB systems having data rates in the hundreds of Mbps. For example, consider a system running at 500 Mbps, with a target BER of 10^{-6} . Such an error rate would produce 500 bit errors per second, in such a high-speed system, and 10^{-6} level of error rate would cause severe system performance degradation.

Instead of battling with the high bit error rates mentioned above, our recommended

approach involves reducing bit error rates to lower rates through first identifying the performance requirements associated with, and then managing, the maximum range of timing synchronization errors. Thus, it became our research goal to determine how small the timing errors must be among the multitude of OFDM data streams, to avoid operation in the asymptotic region, where BER flaring occurs. We propose pushing bit errors to below 10^{-12} before taking advantage of forward error correction (FEC) codes. This way, the maximum reserve is maintained for the FEC hardware to correct for bit errors caused by other than timing synchronization errors.

For the purpose of presentation, this chapter is divided into two sections: analysis of bit synchronization errors and experimental verification using PulsON 200 UWB Evaluation Kit (EVK) hardware.

3.1 Analytical Solutions for BER Performance

At the beginning of our analytical work, we focused on estimating a maximum achievable bit rate, conditioned on timing synchronization bit errors. Through our analysis, we identified timing error effects on bit error rate performance of a high data rate link.

The chosen methodology closely follows the derivations and methods of Lindsey and Simon [2]. The difference between our methods and theirs are that we characterize the synchronization error (λ) to be a normalized timing error resulting from a delay-locked loop. Additionally, we examine bit synchronization for a high data rate stream instead of for symbol synchronization for narrowband applications. Also, we expand our average error probability P_e to below 10^{-12} , since we target this region of interest for applicability to high data rate links.

Finally, our standard deviation of the sync error (σ_λ) and variance of the sync error (σ_λ^2) of the normalized timing error represent ratios of a normalized Unit Interval (UI) of a data bit time period in a data link. A UI is defined to be one bit period or $1/\text{baud rate}$. By utilizing an UI approach, in place of an absolute timing approach, the results of this thesis can easily be applied to ever-increasing data rates for future, thereby increasing the value of the research documented in this thesis.

In the following section, we explain the methodology for our analytical approach that estimated a maximum achievable bit rate, conditioned on bit timing synchronization errors. Our analysis began by obtaining conditional error probability values of the correlation detector conditioned on a timing error; and then we derive conditional error probabilities over a Tikhonov probability density function (pdf) to estimate the probability of bit error at the receiver.

3.1.1 Conditional Error Probabilities

Given that the optimum detector for a known signal is a cross-correlator, the first step in our analysis was to derive for the error probability of the correlation detector conditioned on a bit synchronization error for Manchester, NRZ, RZ and Miller coded data.

Below are the equations, taken from the prior literature, that are used in our analysis to obtain the conditional error probabilities for Manchester, NRZ, RZ, and Miller coded UWB-OFDM data. (See [2] for derivations.)

3.1.1.1 Manchester Coded Data

For a Manchester coded bit stream, the conditional error probability can be realized through the following equation (see table 3.1 for variable definitions):

$$\mathbf{Pe}(\lambda) = \frac{1}{4} \cdot \text{erfc} \left[\sqrt{\frac{\mathbf{Eb}}{\mathbf{No}}} \cdot (1 - 2 \cdot |\lambda|) \right] + \frac{1}{4} \cdot \text{erfc} \left[\sqrt{\frac{\mathbf{Eb}}{\mathbf{No}}} \cdot (1 - 4 \cdot |\lambda|) \right]$$
$$|\lambda| \leq \frac{1}{4}$$
(3-1)

(Where the maximum random value for timing error λ is defined to be $\frac{1}{4}$ for Manchester coded UWB-OFDM data.)

3.1.1.2 NRZ Coded Data

Furthermore, when the bit stream is coded by NRZ data, then the following equation can be used to achieve conditional error probability values:

$$\mathbf{Pe}(\lambda) = \frac{1}{4} \cdot \text{erfc} \left[\sqrt{\frac{\mathbf{Eb}}{\mathbf{No}}} \cdot (1 - 2 \cdot |\lambda|) \right] + \frac{1}{4} \cdot \text{erfc} \left[\sqrt{\frac{\mathbf{Eb}}{\mathbf{No}}} \cdot (1 - 4 \cdot |\lambda|) \right]$$
$$|\lambda| \leq \frac{1}{2}$$
(3-2)

(Where the maximum random value for timing error λ is defined to be $\frac{1}{2}$ for NRZ data.)

3.1.1.3 RZ Coded Data

Next, when the bit stream incorporates RZ coded data, the conditional error probabilities can be obtained with equation (3-3).

$$P_e(\lambda) = \frac{1}{4} \cdot \text{erfc} \left[\sqrt{\frac{\left(\frac{E_b}{N_o}\right)}{2}} \right] + \frac{1}{4} \cdot \text{erfc} \left[\sqrt{\frac{\left(\frac{E_b}{N_o}\right)}{2}} \cdot ((1 - 4 \cdot |\lambda|)) \right]$$
$$|\lambda| \leq \frac{1}{4} \tag{3-3}$$

(Where the maximum random value for timing error λ is defined to be $\frac{1}{4}$ for RZ coded data.)

3.1.1.4 Miller Coded Data

Finally, in the event that Miller coded data is used in the bit stream, equation 3-4 represents an equation that obtains its conditional probability error values.

$$P_e(\lambda) = \frac{1}{2} + \frac{3}{16} \cdot (\text{erf}(a))^2 + \frac{1}{16} \cdot (\text{erf}(b))^2$$
$$- \frac{3}{4\sqrt{\pi}} \cdot \int_0^{\sqrt{2} \cdot c} \text{erf}(x) \cdot \exp \left[-(x - \sqrt{2} \cdot b)^2 \right] dx$$

$$\frac{3}{4\sqrt{\pi}} \int_0^{\sqrt{2}\cdot c} \text{erf}(x) \cdot \exp\left[-(x - \sqrt{2}\cdot a)^2\right] dx$$

$$|\lambda| \leq \frac{1}{4} \tag{3-4}$$

where

$$a := \sqrt{\frac{\left(\frac{E_b}{N_o}\right)}{2}} \cdot (1 - 4 \cdot |\lambda|) \quad b := \sqrt{\frac{\left(\frac{E_b}{N_o}\right)}{2}} \quad c := \sqrt{\frac{\left(\frac{E_b}{N_o}\right)}{2}} \cdot (1 - 2 \cdot |\lambda|)$$

(And where the maximum random value for timing error λ is defined to be $\frac{1}{4}$ for Miller coded data.)

3.1.2 Establishing Average Error Probability at the Receiver

Next in our analysis, after obtaining the stated conditional error probabilities in equations 3-1, 3-2, 3-3, and 3-4 we then averaged them over the probability density function of the bit synchronization errors, to obtain the average error probability P_e at the receiver as determined by equation 3-5.

$$P_e := \int_{-\lambda_{\max}}^{\lambda_{\max}} p(\lambda) \cdot (P_e(\lambda)) d\lambda \tag{3-5}$$

Hence, λ_{\max} reflect the maximum value of which is defined for in the corresponding $P_e(\lambda)$ equations in 3-1, 3-2, 3-3, 3-4, depending on the digital encoding format chosen, and $p(\lambda)$

represents a probability distribution of the normalized timing synchronization error.

Although in [5], a Gaussian timing synchronization error is postulated, we assume a Tikhonov p.d.f. $p(\lambda)$ since this is a more typical characterization of timing errors observed in practical bit synchronizers [18]. Completely characterized in terms of its variance (σ_λ^2) of the normalized timing error, the Tikhonov p.d.f. for the various digital encoded data formats are stated in equations 3-6 and 3-7.

For NRZ data formats, $p(\lambda)$ can be characterized by

$$p(\lambda) = \frac{\exp\left[\frac{\cos 2\pi \cdot (\lambda)}{(2\pi \cdot \sigma)^2}\right]}{I_0\left[\left(\frac{1}{2\pi \cdot \sigma}\right)^2\right]} \quad |\lambda| \leq \frac{1}{2} \quad (3-6)$$

when a Tikhonov PDF is assumed.

Likewise, when employing Manchester, Miller or RZ coding, all of which are base-band techniques that utilize transitions in the middle of the symbol interval, $p(\lambda)$ can be characterized by the Tikhonov PDF in equation 3.7.

$$p(\lambda) = \frac{2 \exp\left[\frac{\cos 4\pi \cdot (\lambda)}{(4\pi \cdot \sigma_\lambda)^2}\right]}{I_0\left[\left(\frac{1}{4\pi \cdot \sigma_\lambda}\right)^2\right]} \quad |\lambda| \leq \frac{1}{4} \quad (3-7)$$

Table 1: Analytical Equation Definitions

Equation Definitions		
Statistical Parameters	Units	Domain or Range
$p(\lambda) = \text{Tikhonov pdf}$	linear	
$\lambda = \text{Timing Sync Error}$	Unit Intervals (UI)	random variable
$\frac{E_b}{N_o} = \text{Energy Per Bit to Noise Ratio}$	linear	0, 1, 2...18
$\lambda_{\max} (\text{Miller}) = \text{maximum } \lambda \text{ value}$	linear	1/4
$\lambda_{\max} (\text{NRZ}) = \text{maximum } \lambda \text{ value}$	linear	1/2
$\lambda_{\max} (\text{Manchester}) = \text{maximum } \lambda \text{ value}$	linear	1/4
$\lambda_{\max} (\text{RZ}) = \text{maximum } \lambda \text{ value}$	linear	1/4
$P_E = \text{Avg error probability}$	linear	
$P_e(\lambda) = \text{Conditional Error Prob}$	linear	
$\sigma_\lambda = \text{Standard deviation of UI}$	Unit Intervals (UI)	Varies
$(\sigma_\lambda)^2 = \text{Variance of UI}$	Unit Intervals (UI)	Varies

By substituting $p(\lambda)$ from equation (3-6) or (3-7) and $P_e(\lambda)$ from equation (3-1), (3-2), (3-3) or (3-4) into equation (3-5) for the a chosen encoded data format (Manchester, Miller, NRZ, RZ), we generated MathCad plots, presented in Figures 12 through 15 (see Chapter 4). These graphs

display average probability of error versus the ratio of the bit energy to the spectral noise power density (E_b/N_0), for the selected UI parameters of normalized timing errors.

With the process described above, we can then estimate the attainable bit error rate for a data link conditioned on normalized timing synchronization errors in Manchester, NRZ, RZ, and Miller coded data. Our results presented in Chapter 4, in Figures 12, 13, 14, and 15, demonstrate the magnitude of Unit Interval (UI) normalized timing error variances that can be accommodated before entering the asymptotic region where BER flaring occurs. For the desired BER, at the point where the curves begin to flare, we identify the maximum allowable timing synchronization error before the use of forward error correction coding. This sets the hardware system timing error for the data link.

With our average error probability graphs, produced using equation (3-5), one can determine how accurate the system timing must be to achieve our goal bit error rate of 10^{-12} . (See Chapter 4, section 4.2).

Later in Chapter 4, we validate our average probability of error results conditioned on timing synchronization errors by using empirical comparisons with laboratory BER measurements. But first, in the following section, we test our methodology by comparing PulsON 200 radio statistical data with its theoretical performance curve.

3.2 Laboratory Measurements using PulsON 200 Radios

Performance Analysis Tool (PAT) software was used in conjunction with two PulsON UWB Evaluation Kit (EVK) transceivers, to gather statistical information about wireless data passed between the two radios. This software is provided with the EVK transceivers to permit

easily assessing link performance. With PAT, we measured the following radio data link statistical parameters:

- Receiver Statistics
- Bit error rate
- Number of bit errors
- Number of bits received
- Number of packets received
- Number of packets dropped
- Effective data rate
- Time (in seconds) that the radio has been running
- Percentage of packets received
- Temperature of the PulsON 200 radio development Module
- Energy per bit
- Effective noise
- Energy per bit to effective noise strength (E_b/N_{eff})
- Transmitter Statistics
- Number of transmitted bits
- Number of transmitted packets
- Time (in seconds) that radio has been running
- Temperature of PulsON 200 radio development Module

3.2.1 Test Procedures

In our test, we conducted range versus data rate measurements in a laboratory environment, which tested the throughput BER over various distances of the UWB transceivers. After configuring the radios for establishing a simple link as outlined in [5], we proceeded with the following steps:

Step 1: Double click on the PAT icon displayed on the laptop or PC monitor

Step 2: When the GUI, similar to Fig. 8, appears on the monitor, select appropriate Radio IP address from the pull down menu and then click the connect button.

Step 3: Once a message appears in the message area that says, “Connected to Radio,” select radio mode, select link rate, and the Eb/Neff mode box from the tabbed form field.

Repeat Steps 1-3 for both radios

Step 4: After a connection has been established for both radios, use measuring tape to separate radios to the desired distance.

Step 5: Next, after performing calibration tests as specified in [5], click start radio on the transmitter radio followed by clicking start on the receiving radio.

Step 6: Analyze statistical data in the statistics frame area, paying close attention to the receiver percentage rate.

Step 7: Vary the gain in the Tabbed Form field area until the receiver percentage rate is 98% or higher. (When radios are far apart, the VGA and the threshold constant, located in the Acquisition Tab, may need to be varied to obtain receiver percentage rate of 98% or higher)

Step 8: Once receiver rate reaches 98% or higher, let the radios run and collect real time statistical data for five to thirty minutes. (Let radio run longer when BER still displays 0)

Step 9: Click Stop radio button on the receiver radio and record radio distance and statistical information from the Statistics Frame

Repeating Steps 1-9 for various separations of the transceivers resulted in the data collected in Table 2.

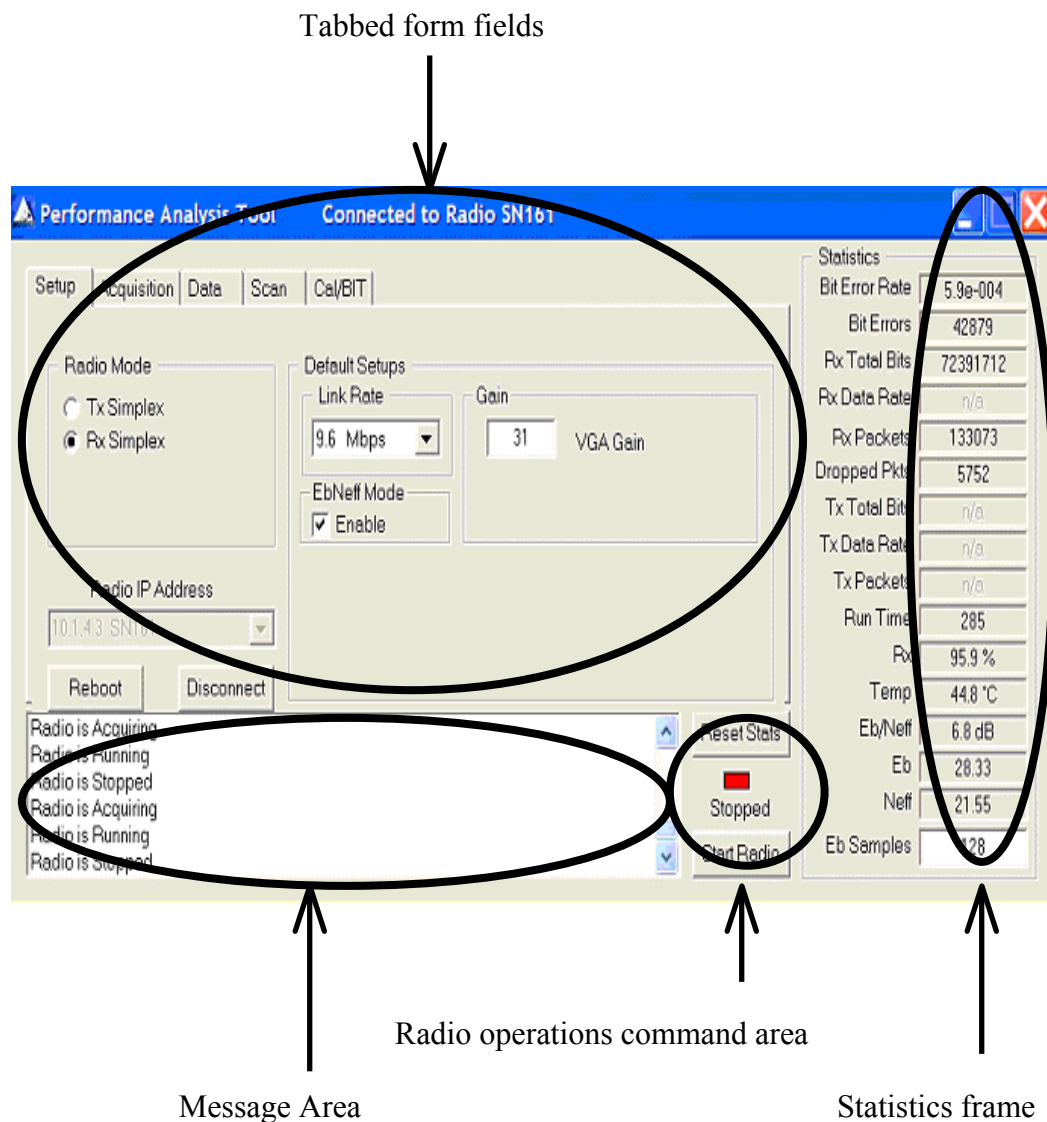


Figure 8: Performance Analysis Tool's graphical user interface for PulsON 200 Receiver.

Since we used the default bi-polar flip modulation while operating the PulsON 200 link (See Figure 9), we calculated a theoretical BER curve for a binary antipodal modulation scheme, to validate our PulsON 200 statistical data.

The theoretical curve of Figure 9 was graphed from the following equations:

$$\text{BER}_{(\text{Flip})} = Q\left(\sqrt{2 \cdot \frac{E_b}{N_{\text{eff}}}}\right) \quad (3-8)$$

where

$$Q(x) = \frac{1}{2} \cdot \text{erfc}\left(\frac{x}{\sqrt{2}}\right) \quad (3-9)$$

and where E_b/N_{eff} ranged from 0 to 14 dB in unit steps.

Development of this curve became necessary to validate the accuracy of the PulsON 200 statistical data.

$$\text{BER}_{(\text{Flip})} := Q\left(\sqrt{2 \cdot \frac{E_b}{N_{\text{eff}}}}\right) \quad (3-10)$$

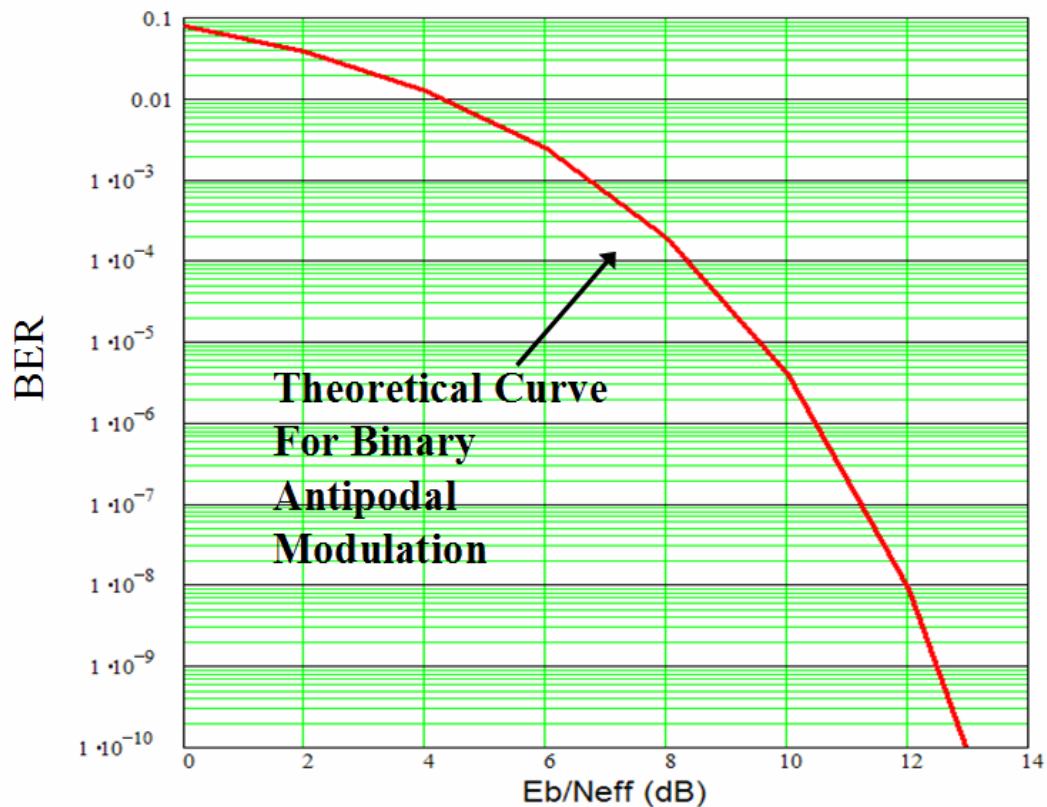


Figure 9: Theoretical BER for PulsON 200 Flip Modulation

In Chapter 4, Figure 17 will display this theoretical curve in conjunction with measured BER data collected during our PulsON 200 test cases. These comparisons will confirm that the received data statistics agree well with its theoretical BER curve; and thus, validates the BER measurements using the PulsON 200 transceiver.

Next, we measured the residual BER of the single-banded PulsON 200 link, and then by extrapolation we determined the equivalent timing uncertainties inherited in a single data stream for estimating the total timing uncertainty in a set of data streams. By measuring the residual BER of a single band link, we determine the irreducible timing errors due to a single path. The

summary result is that timing errors introduce an effect that limits the probability of bit error such that increasing E_b/N_0 (through increasing transmitter power or reducing the range between transceivers) does not improve BER below a limiting error rate.

Chapter 4 presents and discusses the analytical and experimental results developed from the methodologies covered in this chapter. Concluding Chapter Four, we discuss timing accuracies required at a given BER to multiplex (Mux) a set of De-Muxed parallel transmitted data streams utilizing multiple OFDM symbols.

CHAPTER 4 FINDINGS

4.1 Results Overview

As was stated in Chapter 1, the purpose of this study is to determine timing accuracy requirement to avoid entering the asymptotic region of BER flaring at low BERs in the resultant BER curves. To review, our study examined and predicted the flaring in the bit error curves that occur for the different values of normalized timing jitter variances. To validate the study, empirical comparisons were made using experimental results gathered with a pair of PulsON 200 UWB Evaluation Kit Transceivers and PAT. Following are the results from the statistical analysis and the experimental analysis. For the purpose of presentation, this chapter has been divided into four sections. Section 4.2 shows theoretical BER effects due to timing synchronization errors and section 4.3 presents results from the PulsON 200 UWB Radio test cases. In Section 4.4, a relationship is derived with analytical and experimental results from Sections 4.2 and 4.3. Finally, Section 4.5 concludes the chapter with a detailed discussion of how our research results can be applied to designing systems at all data rates and discusses future research for applying this basic theoretical technique to multi-carrier UWB-OFDM systems.

4.2 BER Effects Due to Timing Errors

To provide reliable (distortion less) digital communications, bit synchronization information must be recovered accurately at the receiver. In practical digital communication

systems, we typically transmit only the bit stream and regenerate the bit clock through clock and data recovery (CDR). This is required to properly sample the time-division multiplexed signal (bits) required for making soft (initial) bit decisions. Failure to achieve this perfect synchronism will result in inter-symbol interference and introduce bit errors. These bit errors are caused by distortions and noise in the received bit stream along with imperfections in bit clock regeneration (see Figures 10 and 11). Since our research approach involved reducing bit error rates to as low as possible in UWB systems through identifying maximum allowable timing synchronization errors, we evaluated BER effects due solely to timing jitter. We recognize that this and additional effects are often observed in practical hardware implementations.

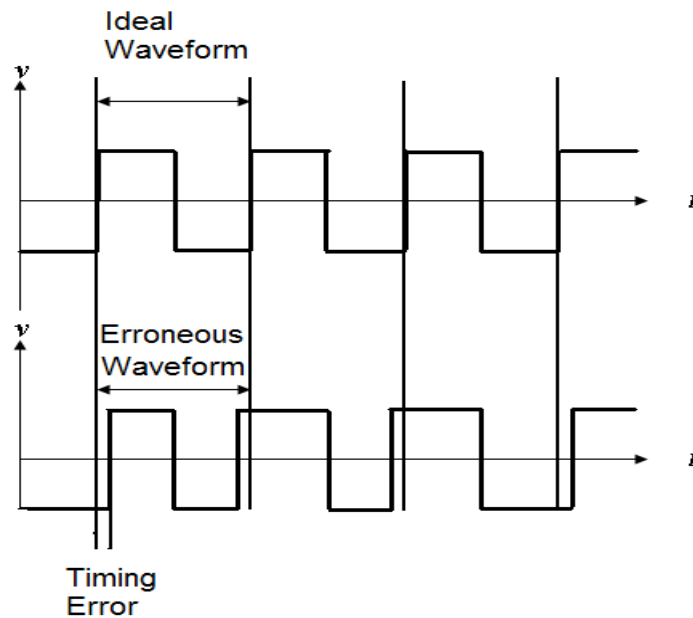


Figure 10: Representation of timing errors in a digital signal

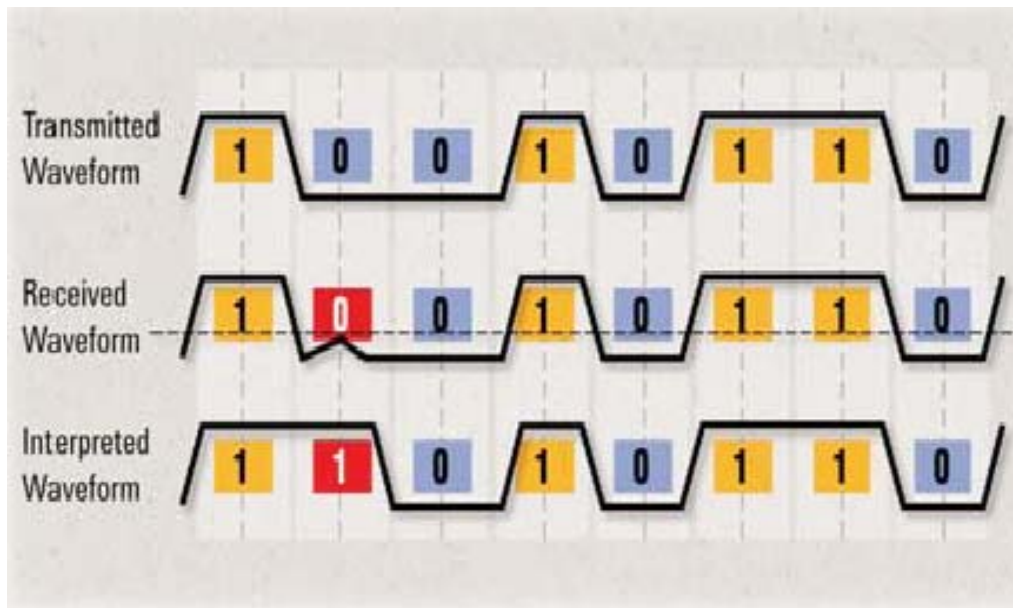


Figure 11: Representation of Distortions in a Digital Signal

In our statistical analysis we considered effects of timing jitter on a system's BER performance. Our first step in this process was to obtain equations that would derive the error probability of the correlation detector conditioned on a bit synchronization error. Then we took this conditional error probability and averaged it over the PDF of the synchronization error, yielding the average error probability at the receiver [2]. As a result, we graphically displayed the process mentioned above through Equations 3-1, 3-2, 3-3, 3-4 from Chapter 3. We plotted these result with MathCAD generated the plots shown in Figures 12, 13, 14 and 15 respectively.

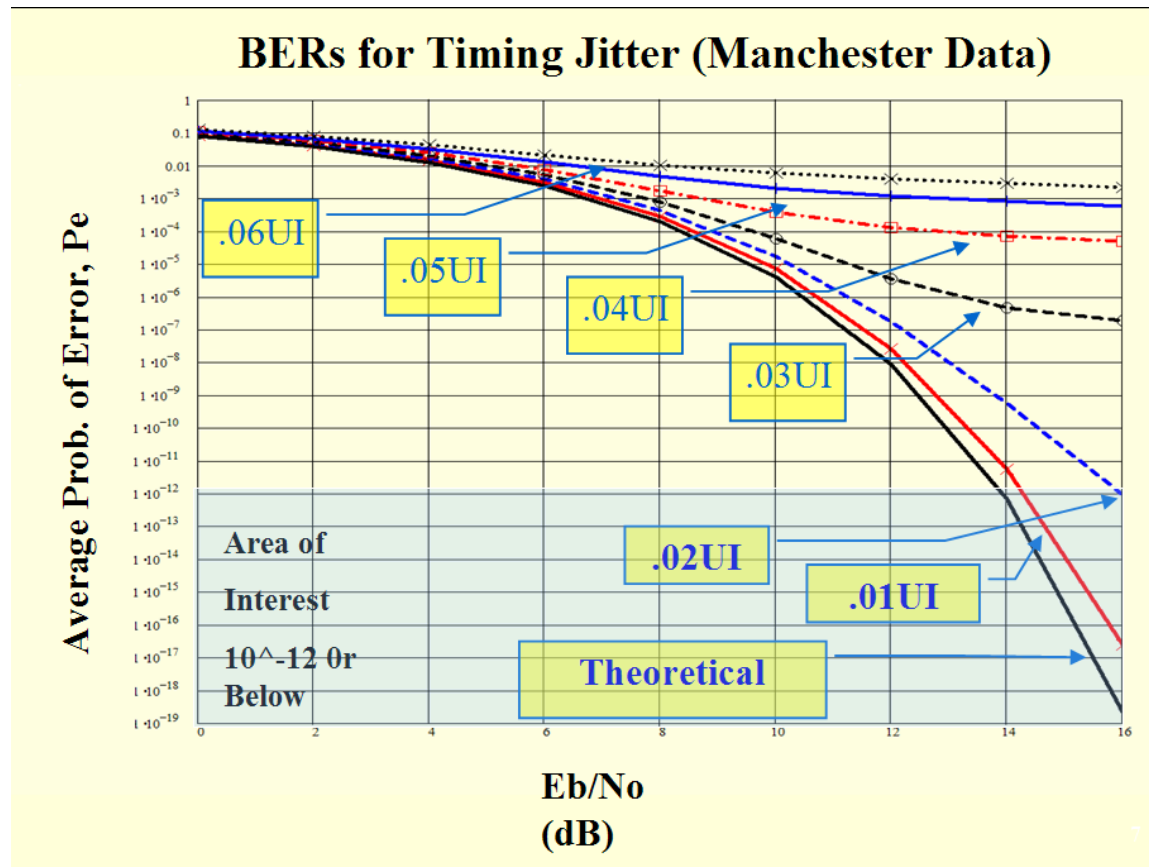


Figure 12: Probability of error for Manchester coded data conditioned on UI timing errors

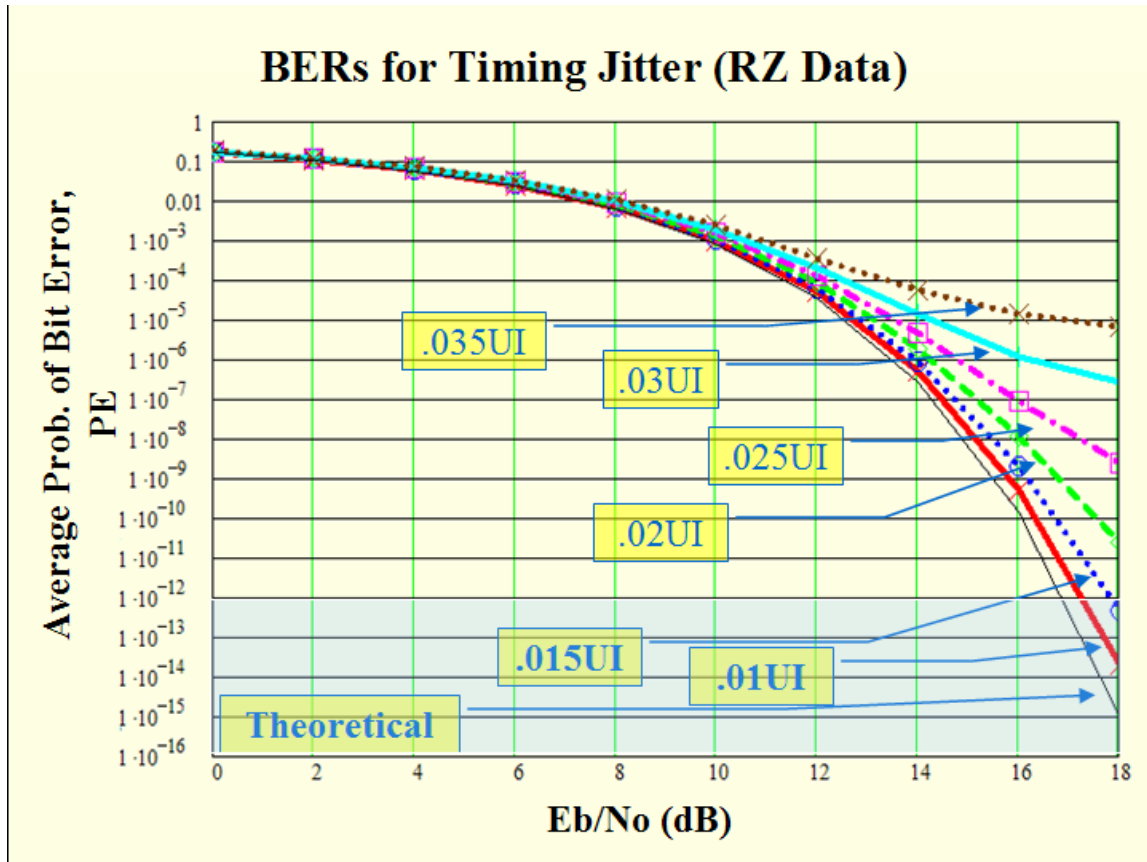


Figure 13: Probability of error for RZ coded data conditioned on UI timing errors

BERs for Timing Jitter (MILLER Data)

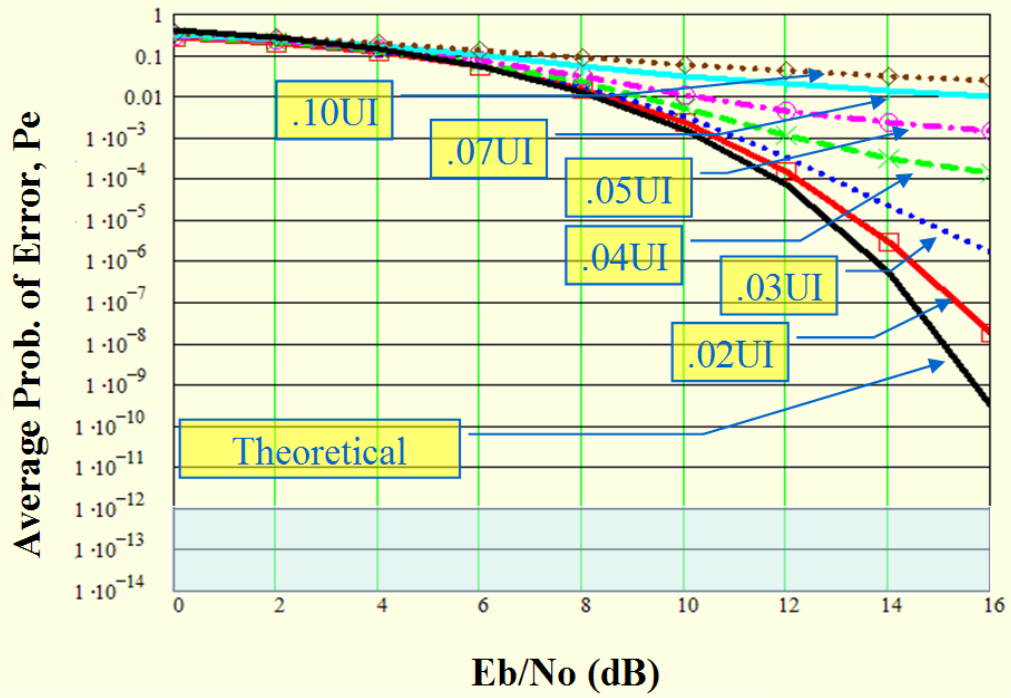


Figure 14: Probability of error for Miller coded data conditioned on UI timing errors

BERs for Timing Jitter (NRZ Data)

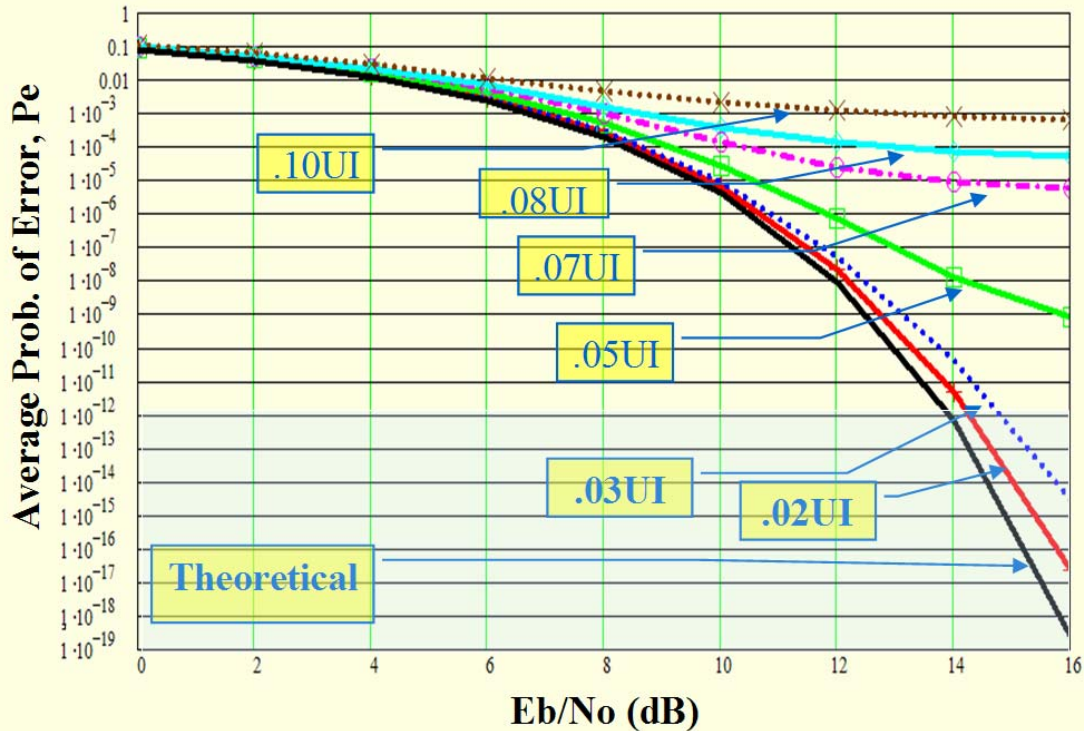


Figure 15: Probability of error for NRZ coded data conditioned on UI timing errors

Analysis of the data from Figures 12 through 15 determined how accurate normalized timing error variances must be to avoid entering the asymptotic region of BER flaring. The flaring is the result of the BER asymptotically approaching the minimum irreducible BER that a system with timing errors can achieve at any arbitrarily high transmitter power level, before incorporating forward error correction codes. With our analysis, we estimate how far the bit errors can be reduced, before the probability of error stops improving (thereby identifying the flaring points of the UI curves). The Manchester coded graph showed the total timing uncertainty

that can be budgeted for a transmitter, de-multiplexer and the receiver clock, and data recovery multiplexing operation. Likewise, graphs shown in Figures 13 through 15 exhibited a similar effect as the Manchester graph, except they may be used for designing systems which incorporate NRZ, Miller, or RZ data in their digital communication system schemes.

In the next section, to apply our statistical analysis, we describe a test case that we developed and performed, to approximate or bound the actual timing uncertainty that exists in PulsON 200 radios. This technique utilizes an easy to implement statistical data collection technique to determine an otherwise difficult-to-determine stochastic jitter performance. It has particular merit whenever making measurements at higher data rates than the test equipment performance has capability for directly assessing jitter performance.

4.3 PulsON 200 Test Case

Following our analyses in the previous section 4.2, we performed experiments to compare our theoretical statistical analysis with actual hardware BER measurements. Our experimental analysis was performed using two PulsON 200 UWB transceivers and Performance Analysis Tool (PAT) software. PulsON 200 radio technology uses a true UWB pulse, as defined by the FCC. Statistical analysis for the transmission BER is made in real time with PAT. Data passed between the PulsON 200 radios allow an evaluator to configure, command, and receive performance of UWB data. (See [5] for specific PAT user operations)

For simplicity, our test cases described in 4.3.3 used the default bi-polar FLIP modulation (see Figure 16) as the choice of modulation. To conduct our analysis, we selected the data rate to be 9.6 Mbps (maximum value available). Although next-generation UWB systems will deliver

data rates in the hundreds of mega bits per second, our experiment confirms that the analysis performed in this thesis, showing flaring due to timing errors, is demonstrated in practice by the PulsON 200 radios. Results of this test case are shown in sections 4.3.3.

In the following section we outline the equipment list and test setup used to conduct the experiment.

Flip Modulation: 2 Symbol States = 1 bit per symbol (pulse)



Figure 16: Flip Modulation (Picture from K.K Lee UWB presentation of Flip-Modulation)

4.3.1 Required Equipment and Test Setup

To conduct test with the UWB radios the following equipment was used:

- Two Time Domain PulsON 200 UWB transceivers
- Two Laptop Computers with PAT software version 3.0
- Category 5 Ethernet connectivity between laptops and UWB radios
- RS-232 serial port connectivity to change radio IP address or view calibration test in

hyper terminal under Microsoft Windows XP

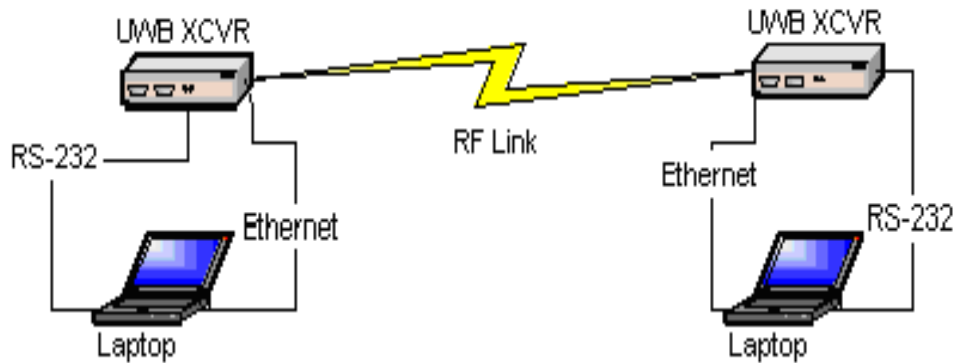


Figure 17: PulsON 200 Evaluation Kit Setup (Figure from [6])

Using the test setup in Figure 17, our objective was to acquire an appropriate volume of digital transmission data to examine a theoretical FLIP modulation BER curve and determine indirectly the timing jitter achieved, consistent with the BER flaring performance actually achieved. Results from these test cases are shown in the following section.

4.3.2 Test Case Results

As described in Chapter 3, measured BER, for UWB digital transmissions, using the PulsON 200 transceivers, was obtained using the PulsON 200 PAT. To obtain sufficient data, we continuously, for stable statistics, recorded transmission characteristics for time periods ranging from approximately 40 to 1600 seconds per distance, per test case, as shown in Table 2.

Then, to confirm our experiment result, we compared the resulting BER to the well-known theoretical formula for binary antipodal modulation:

$$\text{BER}_{(\text{Flip})} = Q\left(\sqrt{2 \cdot \frac{E_b}{N_{\text{eff}}}}\right) \quad (4-1)$$

Notice in Table 2 the collected values for BER and Eb/No. Plotting these measured values, in conjunction with the theoretical BER curves, showed good agreement for values of Eb/No less than 8 dB. This indicates that our collected data is consistent with the theory. However, for data points collected at Eb/No values greater than 8 dB, a gradually asymptotic BER flare evolves around 10^{-4} . This flaring in the BER curve leads us to the discussion in section 4.4, which allows us to assess the approximate timing uncertainty inherent with the PulsON 200 transceivers.

Table 2: PulsON 200 Collection of Data Rate vs. Range Test Cases

RANGE vs. DATA RATE 9.6Mb/s									
PulsON 200 Receiver Test Cases									
Statistics	26.24 feet	26.24 feet	26.24 feet	26.24 feet	100 feet	200 feet	200 feet	330 feet	345 feet
BER	2.90E-04	9.40E-04	1.30E-03	1.40E-04	4.70E-04	1.30E-05	7.00E-04	6.90E-03	1.60E-02
Bit Errors	23426	74866	11031	12275	139660	5647	95761	577526	375518
RX Total Bits	80633312	79511040	86669536	88506624	297129536	425477632	136776832	83864128	23567712
Rx Packets	148223	146160	159319	162696	546194	782128	251428	154162	43323
Dropped Pkts	22	19	218	217	122	7	316	4199	38199
Run Time (Seconds)	304	300	327	304	1119	1603	516	325	167
Rx Rate	99.90%	99.90%	99.90%	99.90%	99.90%	99.90%	99.90%	97.30%	53.10%
Temp.	46.3C	45C	47.8	47.5C	44.5C	45.0C	45.0C	45.0C	46.5C
Eb/Neff (dB)	9.7	8.8	13.3	14.8	7.9	13.6	12.6	6.1	4.5
Eb	31	25.52	34.61	34.9	29.01	33.79	32.22	26.37	25.18
Neff	21.29	16.69	21.35	20.13	21.1	20.22	19.63	20.26	20.72
Eb Samples	128	128	128	128	128	128	128	128	128
VGA Gain	31	23	27	31	24	24	24	31	31
Thres. Const.	80	80	80	80	84	82	82	80	83
log (BER)	-3.54	-3.03	-2.89	-3.85	-3.33	-4.89	-3.15	-2.16	-1.80

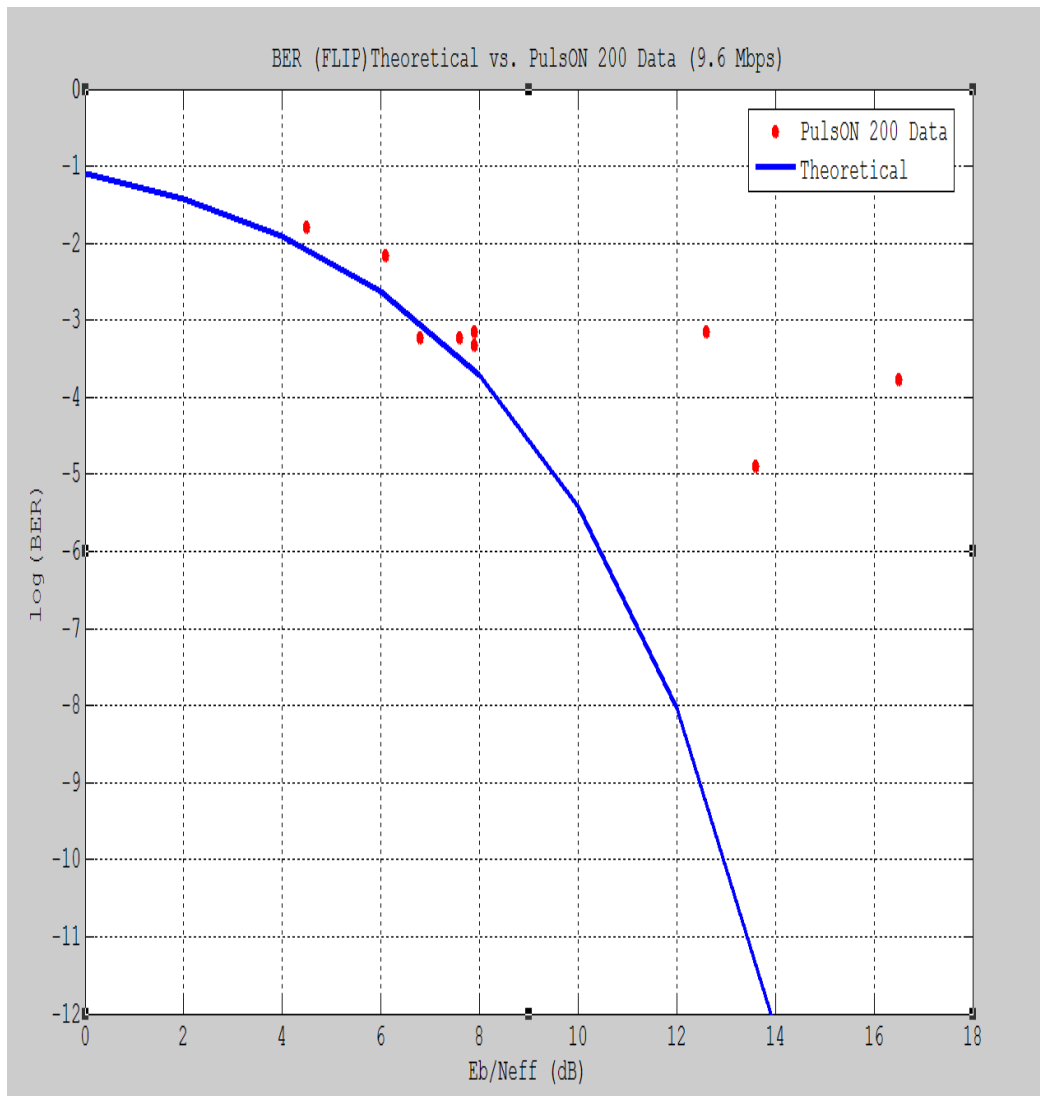


Figure 18: Flip Modulation Theoretical Curve vs. PulsON 200 Data Collected at 9.6 Mbps

4.4 Assessment of Timing Uncertainties

For the purpose of comparing Manchester coded data with experimental data collected in Figure 18, this section plots the Manchester graph in Figure 12 against the experimental data points from Figure 18, to assess the approximate total residual timing uncertainty inherent within

the UWB radio link.

As mentioned in Chapter 3, the summary result is that timing errors introduce an effect that limits the probability of bit error such that increasing E_b/N_0 does not improve BER below a certain error rate. With the experimental data in Figure 18, we found that the probability of error stopped improving in approximately the 10^{-4} region. After we collected sufficient data to identify the BER asymptote, we then extrapolated these data points and inserted them into our Manchester theoretical graph as seen in Figure 19. Since our Manchester graph shows probability of error conditioned on normalized timing synchronization error, we were able to identify the normalized unit interval value of timing error in the PulsON 200 radio. The black solid curve represents theoretical values (zero timing error), while the other curves range from normalized variances of 0.055 UI to 0.030 UI, in 0.005 step sizes. Our extrapolated data points from our PulsON 200 experiment is also represented on the graph by the blue and red circle-shaped points. (Different colors represent statistical data collected in two different environments) As seen in Figure 19, experimental values surrounded the “best fit” curve that represents timing error of 0.04 UI. From this analysis, we identify the normalized unit interval value of timing error in the PulsON 200 radio to be 0.04 UI, since this jitter curve best fits our experimental data points.

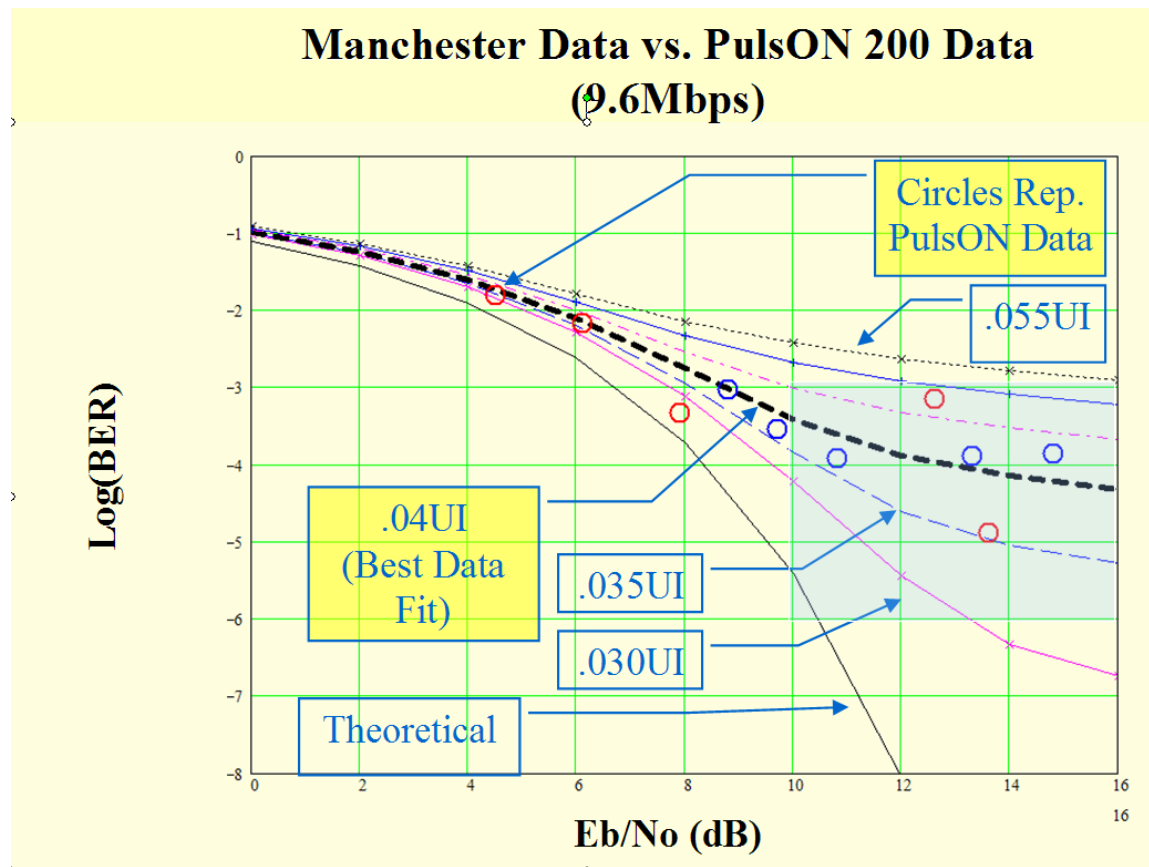


Figure 19: Manchester’s Average Probability of Error Curves with extrapolated PulsON 200 Data

In conclusion, we estimated the normalized timing uncertainty for the PulsON 200 radio, due to timing jitter, through an easily measured indirect technique, instead of a difficult-to-make direct technique at high data rates. We are able to use this same concept to predict how much timing uncertainty should be budgeted for designing future high data rate (hundreds of Mbps) UWB systems.

4.5 Analysis of Effects on UWB-OFDM System with High Data Rates

Predicting how much timing uncertainty that should be used in designing future high data rate systems in the multiple hundreds of mega bits per second can be estimated with our unit interval (UI) approach. In this thesis, we have defined the unit interval to be the reciprocal of the data symbol rate. For example, in a system running at 10 Mbps, one unit interval bit period is equal to 1/10 Mbps. In this case, one unit interval is equivalent to 0.10 μ secs. For systems running at different speeds, one unit interval may still be determined by equating one nominal bit symbol period for its given signal speed to a unit interval. Therefore, rather than using the absolute timing approach, we used the UI approach so that our analysis can be used in approaching UWB-OFDM systems operating at higher data rates.

Likewise, normalized (with respect to a bit time) timing error UI's are represented as the timing synchronization errors analyzed throughout this thesis. These values are small percentages of a unit interval, which define the standard deviation of a normalized timing error in terms of UI random timing jitter. A 0.02 UI random timing error measurement means that the standard deviation statistic of a bit period deviation is around 2% of the ideal bit period time. Through utilizing a Unit Interval approach, in place of an absolute timing approach, the results of this thesis can easily be applied to ever-increasing data rates of future UWB-OFDM data links.

The results in this thesis pertain to a reference UWB-OFDM system, yet evolving UWB-OFDM systems will likely use a multi-band approach. Once the bit timing synchronizations are corrected using the approach discussed in this thesis where we analyzed the timing bit errors per symbol for two OFDM symbols, then further research can be applied to analyze the timing symbol synchronization errors for multiple symbols in a multi-band UWB-OFDM system.

Assessment of timing uncertainty of realistic symbol timing in the evolving multi-band UWB-OFDM may be realized through the same approach used to assess the bit time synchronization timing uncertainties in the reference UWB-OFDM system. Qualitatively, the main results from this thesis remain valid for the evolving multi-band UWB-OFDM systems. In Chapter 5 we discuss recommended further research in the multi-band UWB-OFDM systems.

CHAPTER 5 CONCLUSION

5.1 Summary of Results

This thesis has developed theoretical equations for estimating BER effects due to timing uncertainties among multiple OFDM channels. We considered UWB-OFDM systems which were coded by Manchester, Miller, RZ, and NRZ data. Since we proposed pushing bit errors to below 10^{-12} before using forward error correction codes, we focused on identifying the maximum timing synchronization errors allowable for a selected BER of the above encoding types. In this manner, the maximum reserve could be maintained for the FEC to correct for errors caused by instances other than timing errors. So, we were able to identify how accurate timing must be to avoid introducing the asymptotic region of BER flaring at probability of errors of 10^{-12} or below. According to our analysis, for Manchester data formats, to obtain a P_e of 10^{-12} or below, timing accurate instances should be budgeted at a maximum, 0.02UI. NRZ coded data timing accuracy should be budgeted at a maximum of 0.04UI. RZ data formats should be budgeted at a maximum of 0.015UI. Unfortunately, Miller Coded data was not able to achieve a probability of error of 10^{-12} , therefore we found that this data format could not be used for our approach. The above values provide an estimate of the timing accuracy required for a given BER performance to MUX a set of parallel transmitted, De-Muxed data streams, utilizing multiple OFDM symbols transmitted within multiple sub-bands.

PulsON 200 “EVK” was used to make measurements of a single sub-banded data stream,

to determine the equivalent timing uncertainties inherited in a single data stream for estimating the total timing uncertainty in a set of OFDM data streams. With the laboratory BER measurements performed, we were able to use our analytical solutions to determine the approximate amount of timing uncertainty budgeted for the radios. This test case demonstrated that our analytical and experimental solutions agree well. As a result, we are able to assess how much timing uncertainty that can be budgeted for UWB systems; and using our unit interval approach this could be applied to all other high data rate systems.

5.2 Recommendations for Future Work

Recommendations for continuing this research would include determining the probability of error effects due to secondary causes other than timing errors. These secondary sources of degradations may include probability of error effects due to phase noise, multi-path propagation effects, noise figure, etc.

In addition, looking at timing error effect along with the secondary sources of— degradations mentioned above should be examined for multi-banded UWB-OFDM. Instead of examining the bit synchronization of the data stream as we examined in this thesis, the idea can be expanded to examine the symbol synchronization effects. This would involve not only timing error effect, but also frequency error effect of the multiple OFDM symbols and the requirement to multiplex the symbols back together in ways that minimize inter-symbol interference and inter-carrier interference, while lowering bit error rates down below 10^{-12} .

APPENDIX A
PERFORMANCE ANALYSIS TOOL

A.1 PAT Statistics Frame Area

The Statistics Frame Area shown on the right side of the PAT shows key PulsON 200 radio performance measurements (See Figure 20) While observing performance parameters of the connected radio, we were able to analyze: BER, Bit errors, Receiver Total Bits, Receiver Data Rate, Receiver Packets, Dropped Packets, Transmitter Total Bits, Transmitter Data Rate, Transmitter Packets, Run Time, Receiver percentage Rate, Radio Temperature, Energy Per Bit/ Effective Noise (dB), Energy Per Bit, Effective Noise, and Number of Samples Over which Eb is computed.

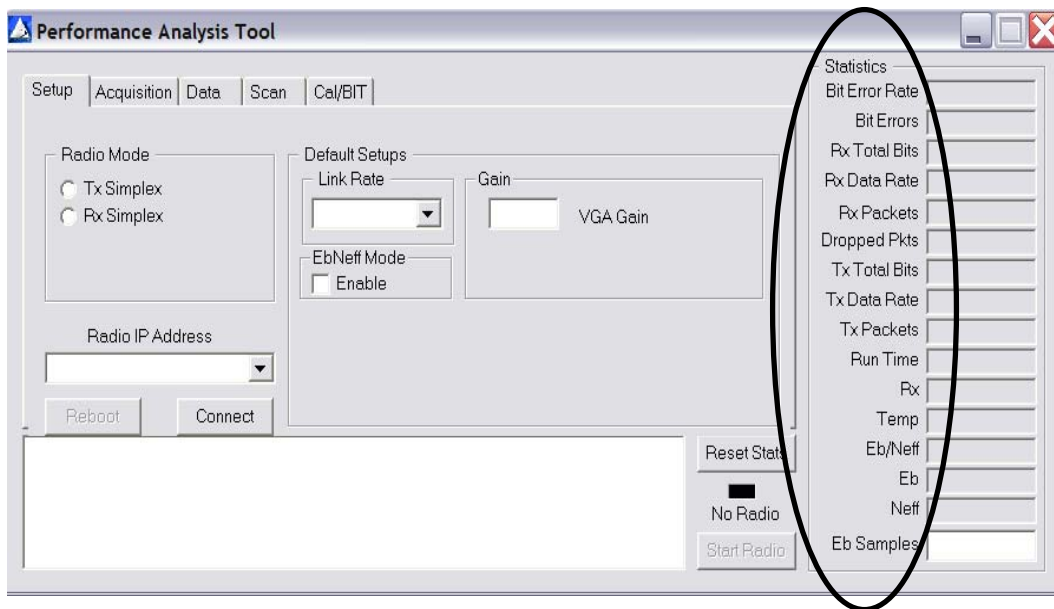


Figure 20: PAT Statistics Frame Area

The above statistical parameters were defined and computed automatically with the PAT by the following (As outlined in [5]):

Bit Error Rate- The ration between the number of bits in error and the total bits received, computed as: $BER = \text{Bit Errors} / \text{Rx Total Bits}$ (BER)

Bit Errors-Total number of bit errors detected by comparing the received bit pattern with the known transmitted bit pattern.

RX Total Bits- Total number of payload bits received. This number does not include the overhead of the acquisition preamble or the packet header.

RX Data Rate- Rate at which data is being received:

$\text{Rx Data Rate} = \text{Rx Total Bits} / \text{Run Time}$ (Effective data rate)

RX Packets- Total number of packets received

Dropped Pkts- Total number of packets whose number is not sequential to the packet last received, computed as:

Dropped Packets= Dropped Packets + (current packet number – last packet number-1)

TX Total Bits- Rate at which data is being transmitted, computed as:

Total number of payload bits transmitted.

TX Data Rate- Rate at which data is being transmitted, computed as:

(# of packets received/# of packets sent) x 100

Temp- temperature of the temperature sensor on the PulsON 200 Development Module

E_b-Energy per bit, computed as:

$$E_b := 10 \log\left(\frac{m^2}{N}\right)$$

where

$$m := \frac{1}{R} \cdot \sum_{i=1}^R (r_i)$$

N= 1 for Flip modulation, 2 for QFTM, 4 for QFTM4

r= raw positive ramp value with calibrated DC offset applied

R= number for ramp

N_{eff}- Effective noise computed as:

$$N_{\text{eff}} := 10 \log(2 \sigma^2)$$

$$m := \frac{1}{R} \cdot \sum_{i=1}^R (r_i - m)^2$$

R= number for ramp

r =raw positive ramp value with calibrated DC offset applied (when running a normal link)

OR

=raw positive or negative ramp with calibrated DC offset applied (when capturing Ambient RF)

Eb/Neff- Energy per bit/ Effective Noise, computed as:

$E_b - N_{eff}$ (dB)

Eb Samples- This value is the number of samples over which Eb is computed. The default number of samples is 512 and must follow the rule: $2 \leq \text{Eb Samples} \leq 4095$.

A.2 PAT Range vs. Data Rate Test Cases

The Range vs. Data Rate Test used in this thesis tested throughput rates over various distances between the UWB transceivers. Test Cases performed during our testing proceedings are shown below through screen shots taken from the PAT.

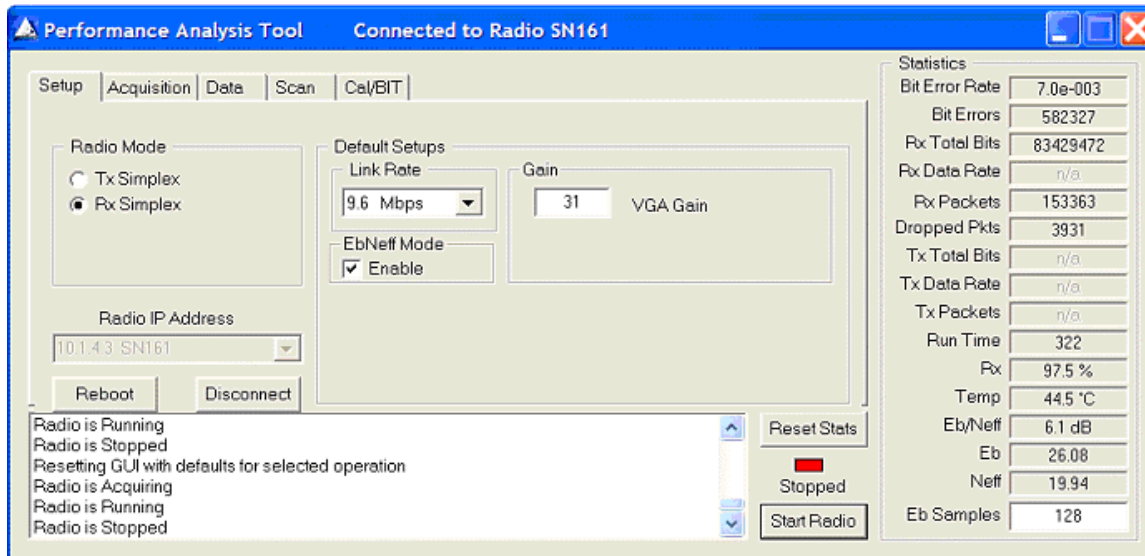


Figure 21: PAT Test Case @ 330 feet distance

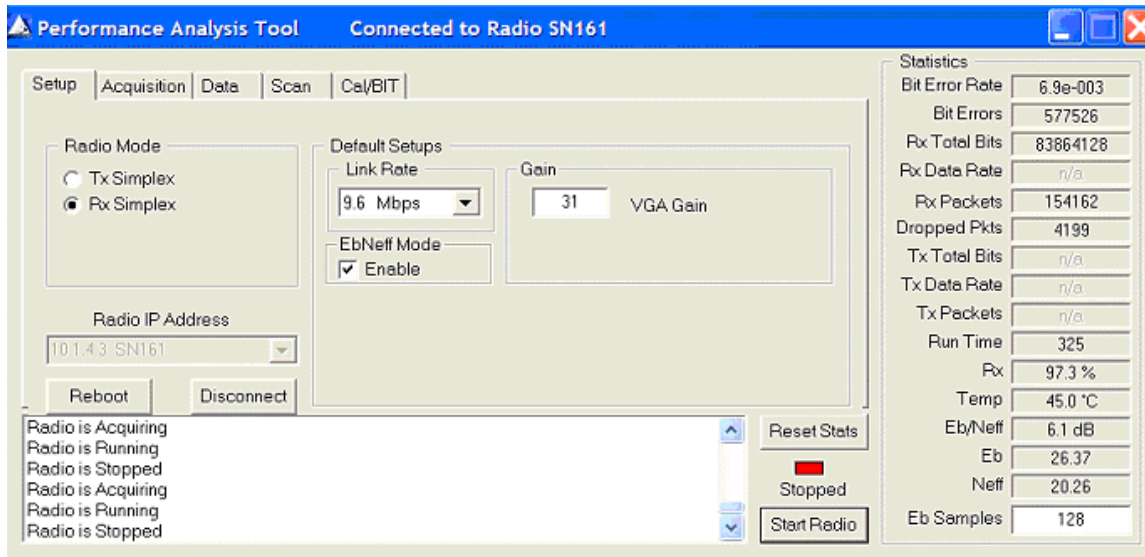


Figure 22: PAT Test Case @ 330 feet distance

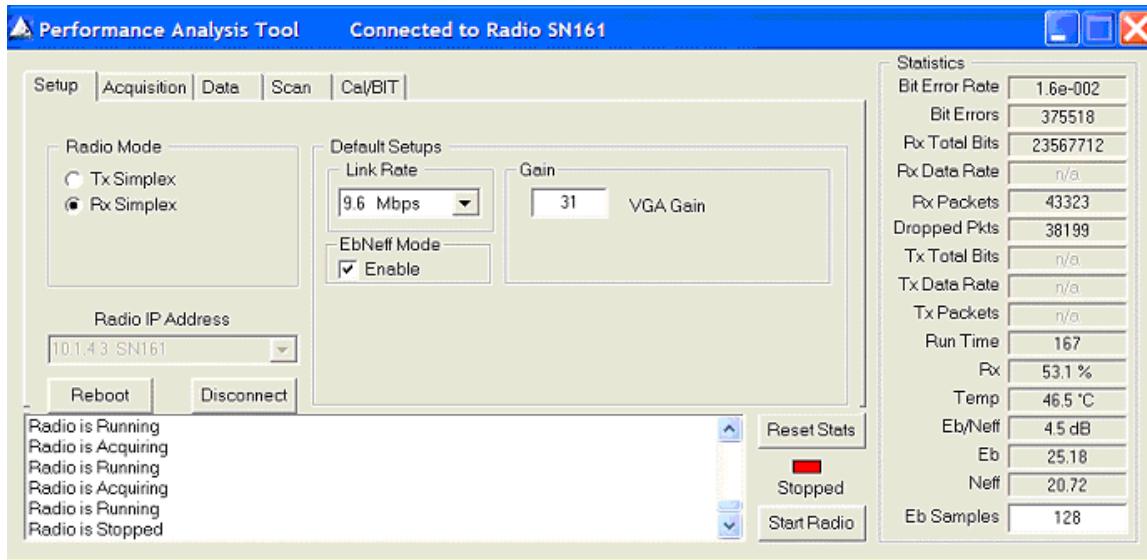


Figure 23: PAT Test Case @ 345 feet distance

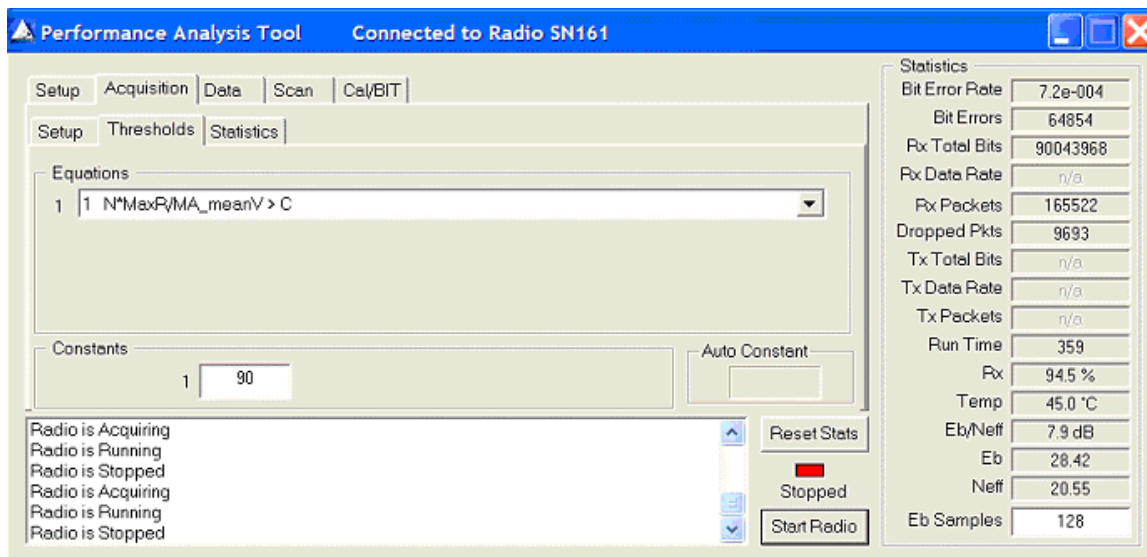


Figure 24: PAT Test Case @ 300 feet distance and VGA 31

By extracting the Eb/Neff value and its corresponding BER from each test case above, we were able to plot and analyze the data and make hypotheses throughout this thesis.

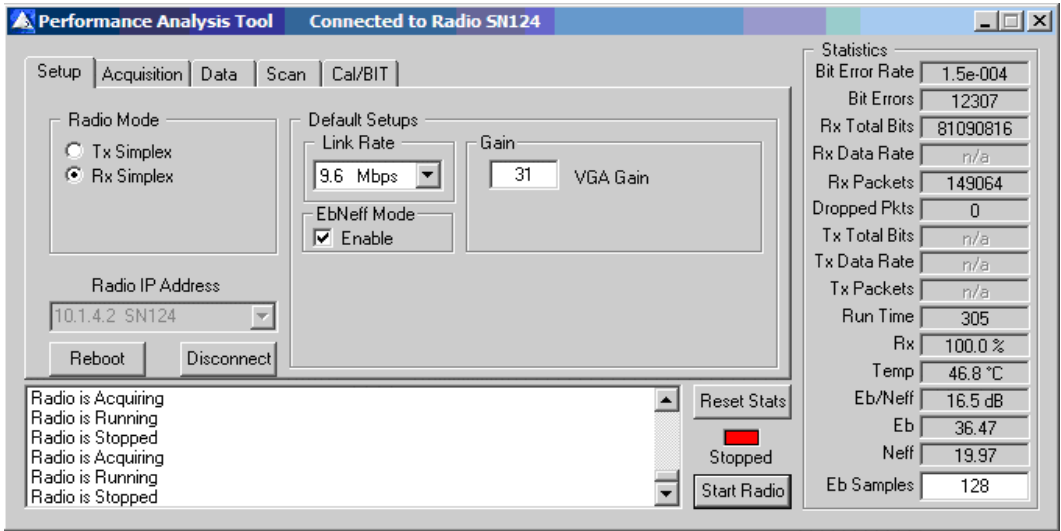


Figure 25: PAT Test Case @ 16.40 feet or 5 meters distance

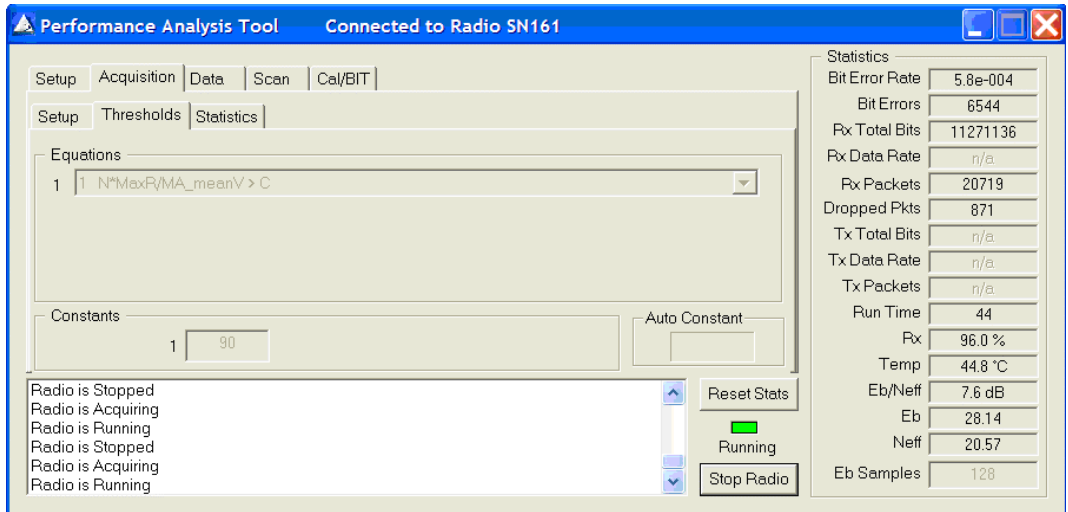


Figure 26: PAT Test Case @ 300 feet distance

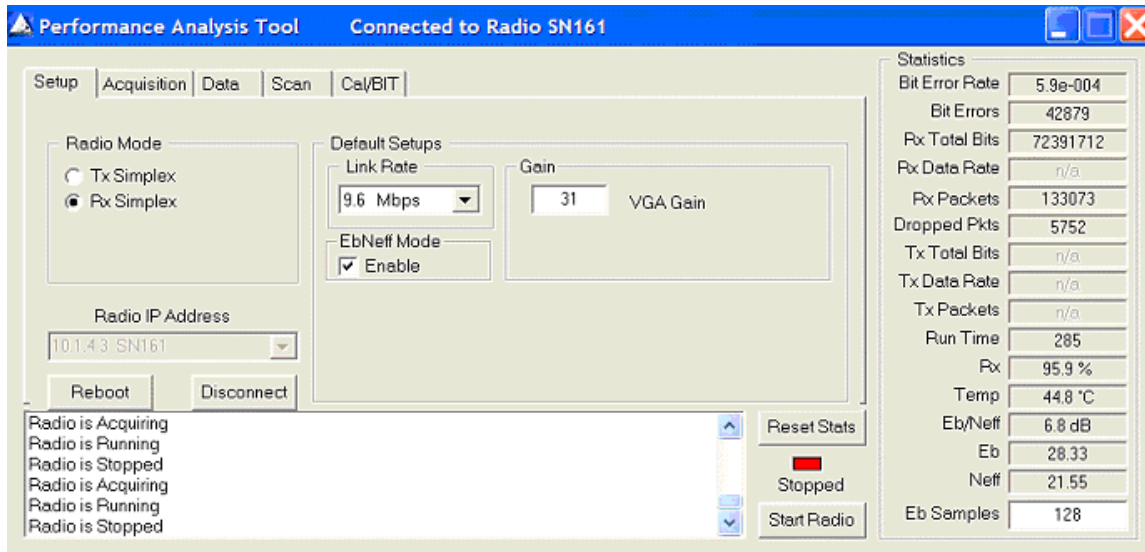


Figure 27: PAT Test Case @ 300 feet distance

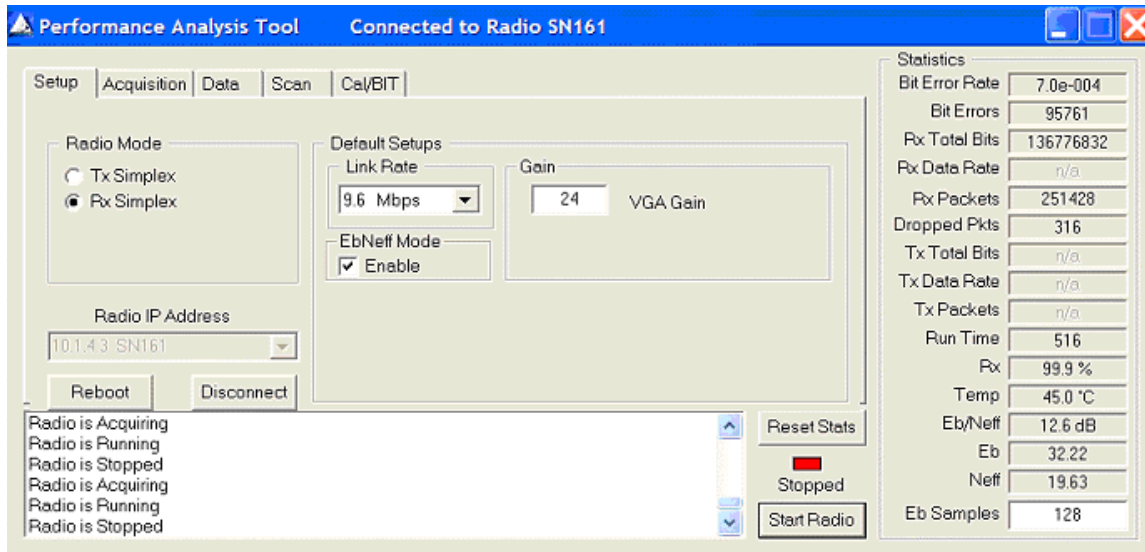


Figure 28: PAT Test Case @ 200 feet distance

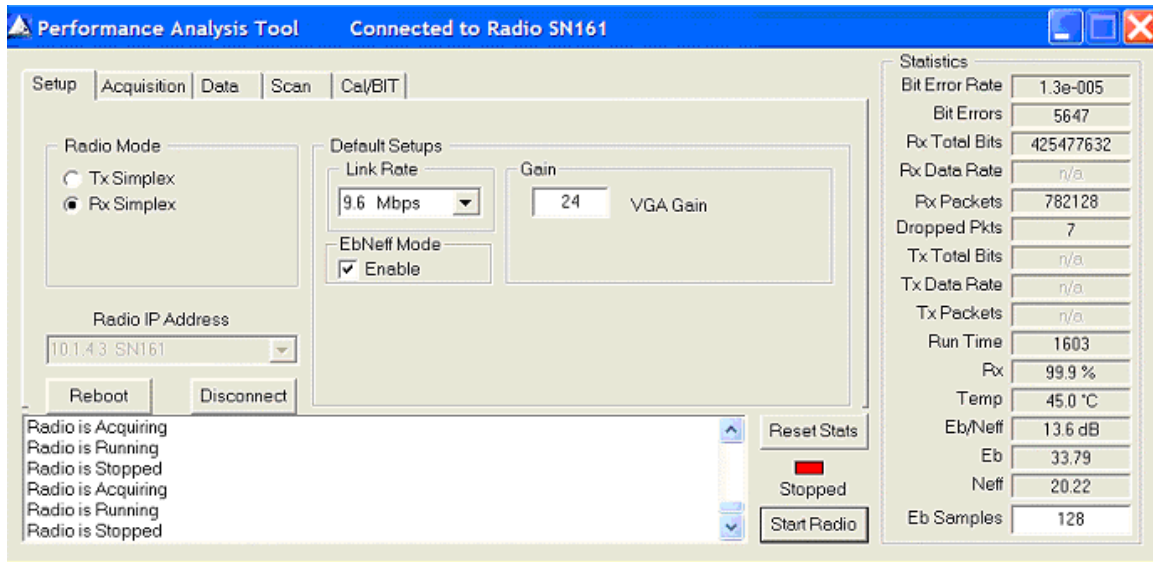


Figure 29: PAT Test Case @ 200 feet distance

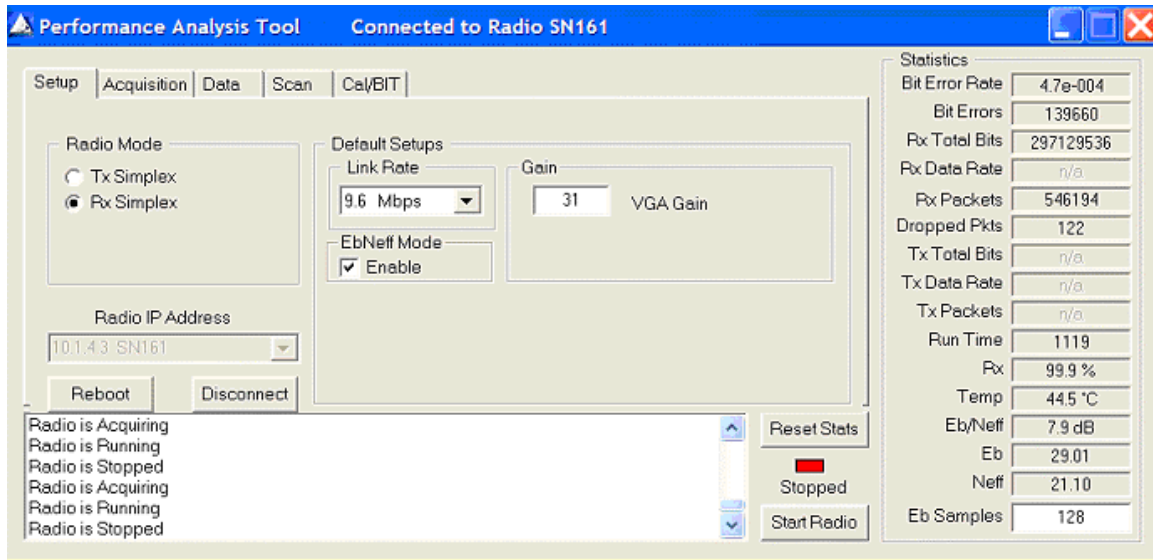


Figure 30: PAT Test Case @ 100 feet distance

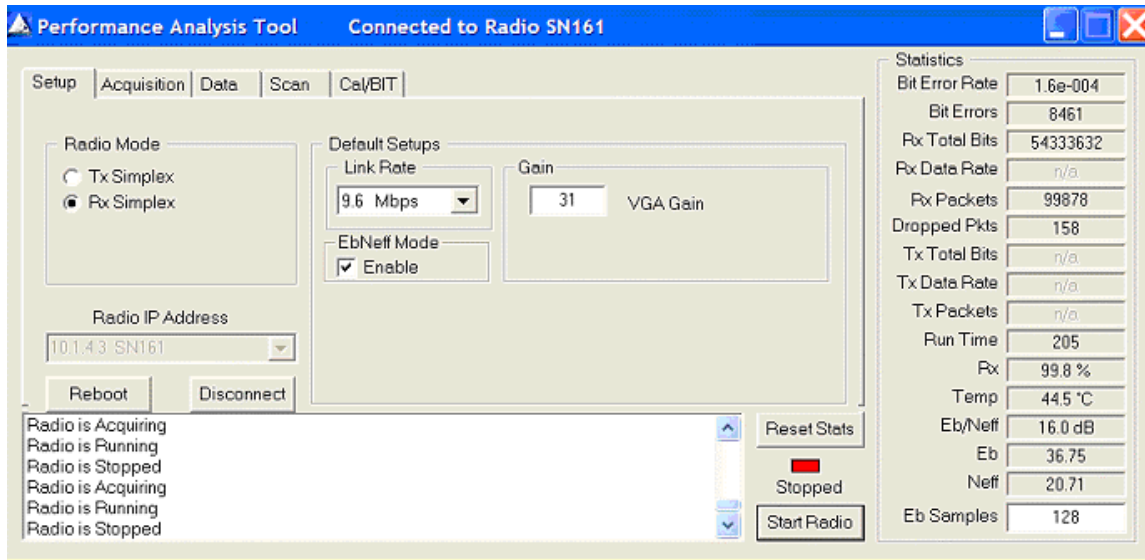


Figure 31: PAT Test Case @ 10 feet distance

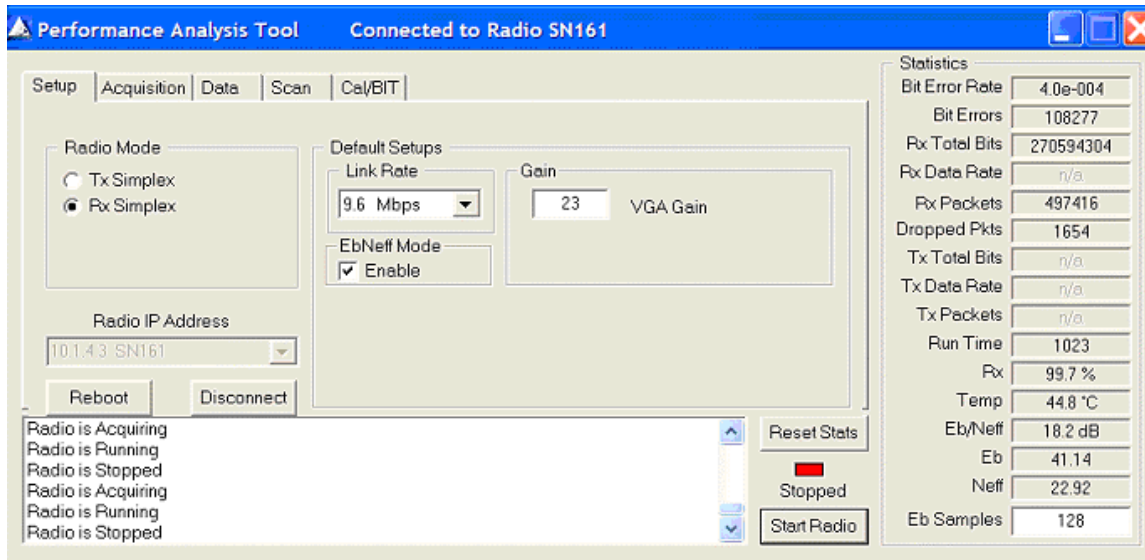


Figure 32: PAT Test Case @ 5 feet distance

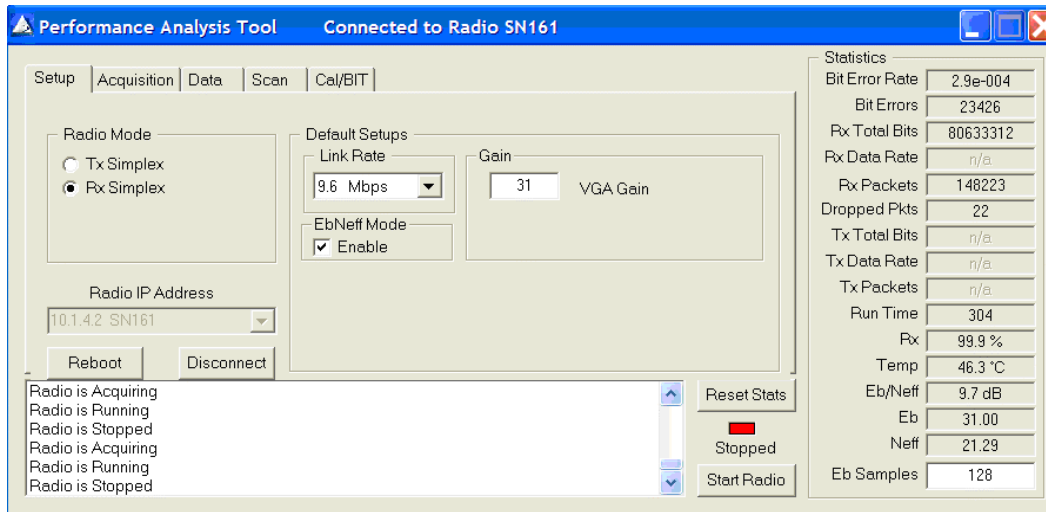


Figure 33: PAT Test Case @ 26.24 feet or 8 meter distance

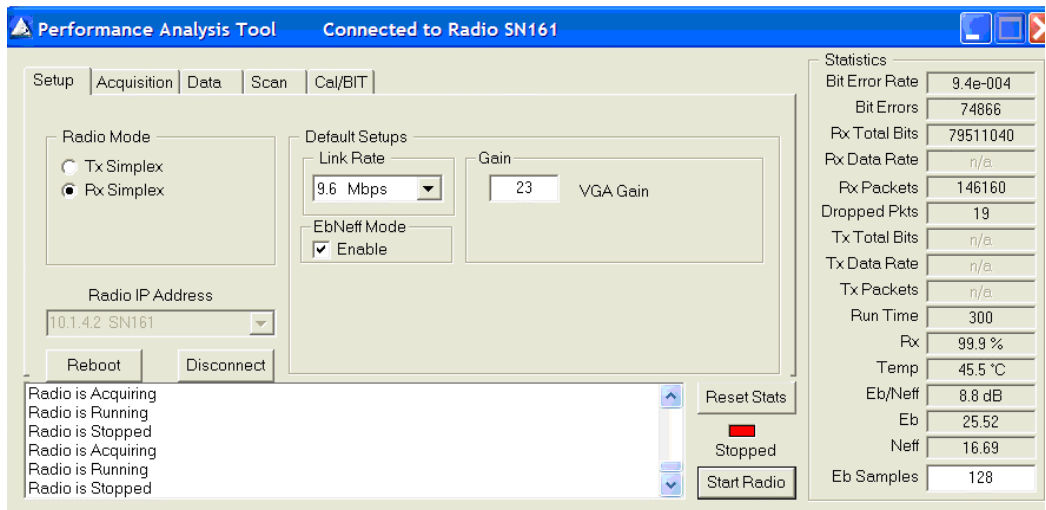


Figure 34: PAT Test Case @ 26.24 feet or 8 meter distance

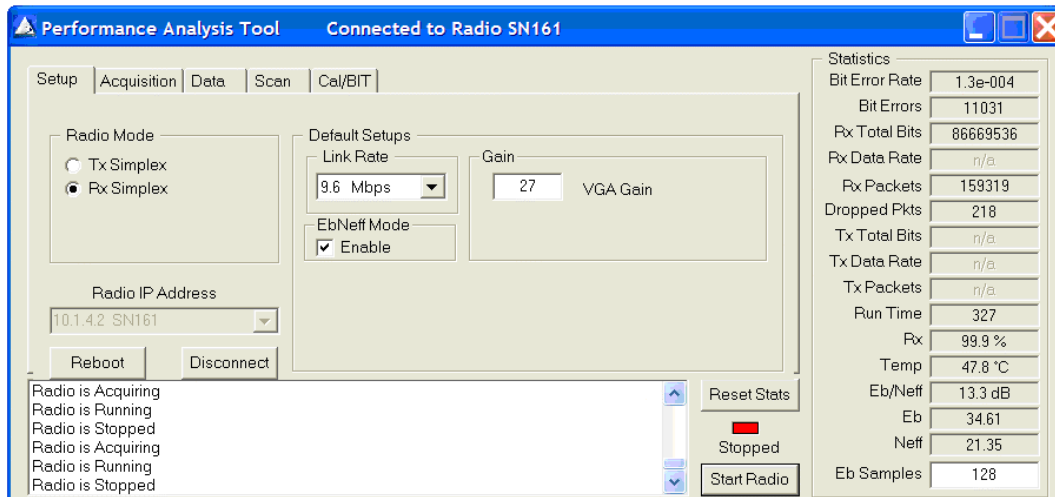


Figure 35: PAT Test Case @ 26.24 feet or 8 meter distance

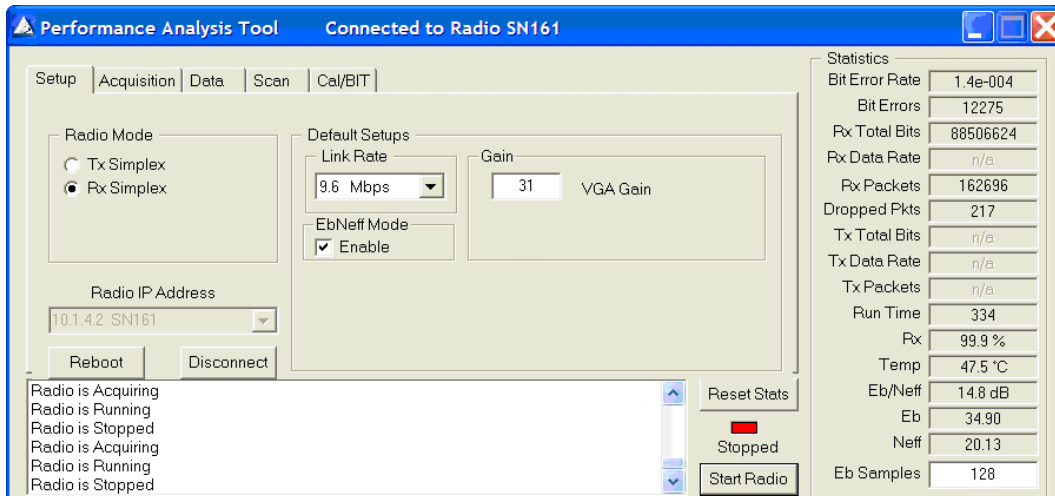


Figure 36: PAT Test Case @ 26.24 feet or 8 meter distance

APPENDIX B
DIGITAL SIGNALING FORMATS

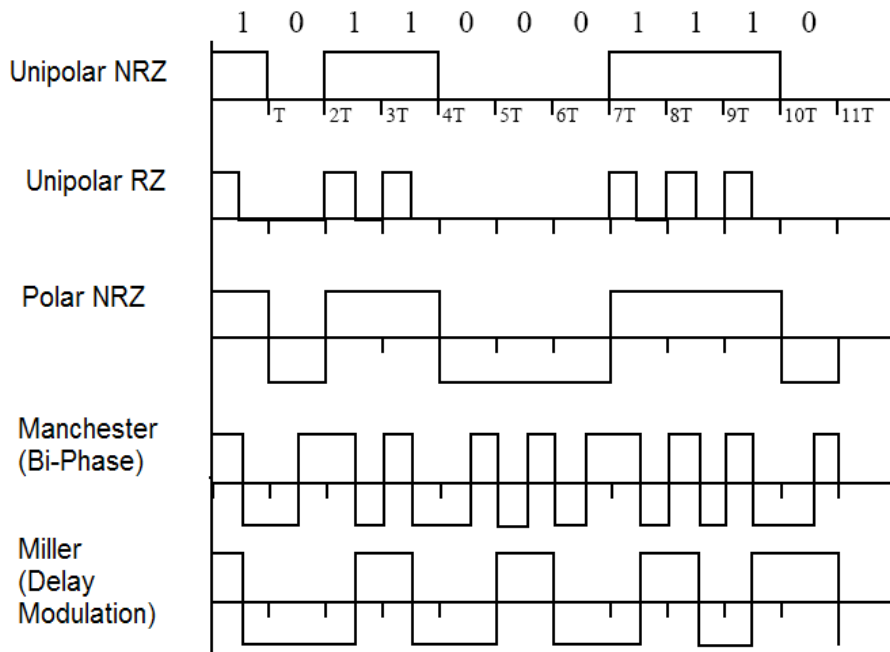


Figure 37: Binary Line Coding

Binary 1's and 0's may be represented by various binary line codes. Some of the more popular formats are shown in Figure 37 and are defined as follows.

Unipolar NonReturn to Zero (NRZ) Signaling is a positive logic unipolar signaling where the binary 1 is represented by a high level and a binary 0 by a zero level. This type of signaling is also called on-off keying and is of the NRZ type since the high level does not return to zero during the binary 1 signaling intervals.

Unipolar Return to Zero (RZ) is a unipolar waveform in which a binary 1 is represented by a high level over half of a bit period and then returns-to-zero. The binary 0 is represented by a zero level.

Polar NRZ is binary 1's and 0's that are represented by equal positive and negative

levels. This type of waveform is also said to be of the NRZ type.

Manchester coding is where each binary 1 is represented by a positive half-bit period pulse followed by a negative half-bit period pulse followed by a positive half-bit period pulse. This is called split-phase encoding.

Miller line code is where a binary 1 is represented by a transition at the mid-bit position, and a binary 0 is represented by no transition at the mid-bit position. If a 0 is followed by another 0, however, the signal transition also occurs at the end of the bit interval, that is, between the two 0s.

APPENDIX C
RELATIONSHIP BETWEEN E_b/N_0 AND S/N

Ways in which we measure performance of communication systems depend on the probability of error (Pe) or the bit error rate (BER) performance. These two statistical parameters measurement probability of making a mistake of identifying a correct symbol, or bit at the receiver. In the telecommunications industry we measure the probability of error and the signal strength by plotting Pe verse average signal power over average noise power (SNR), or verse (vs.) energy per bit over noise spectrum density (Eb/No) of a given system. SNR is important in measuring analog systems, whereas we use Eb/No in place of SNR when analyzing a digital system. Eb/No can be viewed as a normalization (to a bit period) to the SNR.

In digital systems we plot Pe vs. Eb/No instead of Pe vs. SNR because digital symbols exist over a bit period (Tb) rather than existing over what can be thought of as existing over a long time period as seen in analog signals. The relationship between SNR and Eb/No is as follows.

Eb is equivalent to the signal power (S) multiplied by the duration time T of a rectangular pulse (in seconds). Therefore,

$$\frac{E_b}{N_o} = \frac{S \cdot T}{N_o}$$

Where No is the noise spectral density, which implies that [22]:

$$\frac{E_b}{N_o} = \frac{S}{N_o \cdot \left(\frac{1}{T}\right)}$$

Since a rectangular pulse of duration T seconds has amplitude spectrum $AT\text{sinc}Tf$ and its bandwidth is roughly measured by $B_p = 1/T$ [8], then,

$$\frac{E_b}{N_o} = \frac{S}{N_o \cdot B_p}$$

where B_p is sometimes referred to as the bit-rate bandwidth.

Relating noise power spectral density (N_o) to noise power (N):

$$N_o = \frac{N}{BW} \quad [22]$$

where BW is the input noise bandwidth, then E_b/N_o relates to S/N by [15]:

$$\frac{E_b}{N_o} = \frac{S}{N_o \cdot B_p} = \frac{S \cdot BW}{N \cdot B_p} = \frac{S \cdot BW \cdot T}{N}$$

In the above equation, we show the bit energy-to-noise density ration E_b/N_o , which is

equal to the ratio of the signal power S and the noise power N in a bandwidth equal to the bit rate bandwidth $B_p = N_o/T$ [15].

Ideally, when measuring performance in digital communication systems we like to see low errors achieved at low energy per bit.

APPENDIX D
Q-FUNCTION, ERF, AND ERFC

Q-function is described as the tail integral of a unit Gaussian PDF. Represented mathematically:

$$Q(x) = \frac{1}{\sqrt{2\pi}} \cdot \int_x^{\infty} e^{-\frac{t^2}{2}} dt$$

Other functions that are closely related to Q(x) include error function erf and complimentary error function erfc.

$$\text{erf}(x) = \frac{2}{\sqrt{\pi}} \cdot \int_0^x e^{-t^2} dt = 1 - \text{erfc}(x) \quad [23]$$

and

$$\text{erfc}(x) = \frac{2}{\sqrt{\pi}} \int_0^{\infty} e^{-t^2} dt = 1 - \text{erf}(x) \quad [23]$$

Relationships between Q(x), erf, and erfc can be shown by the following:

$$Q(x) = \frac{1}{2} \cdot \left(1 - \text{erf}\left(\frac{x}{\sqrt{2}}\right) \right) = \frac{1}{2} \cdot \text{erfc}\left(\frac{x}{\sqrt{2}}\right)$$

In scientific literature there may be a few variations of erfc which differ by definition. For example in literature reference by Harry Van Trees, the erfc is defined differently than the classical mathematical definition in material referenced by Abramowitz and Stegun. We use the

classical definition, since it appropriately approximates the probability of a bit error.

REFERENCES

1. Harada, Hiroshi, Prasad, Ramjee, Simulation and Software Radio for Mobile Communications, Artech House, 2002.
2. Lindsey, W. C. and Simon, M. K., Telecommunication Systems Engineering, Prentice-Hall, Inc., 1973.
3. Athaudage, Chandranath, "BER Sensitivity of OFDM Systems to Time Synchronization Error," Proceedings of the IEEE, vol.1 (2002): 42-46.
4. Heiskala, Juha and Terry, John PhD, OFDM Wireless LANs: A theoretical and Practical Guide, SAMS Publishing, 2002.
5. "PulsON 200 Evaluation Kit Users' Manual," Time Domain Corporation, 2001-2002.
6. Bastin, Gary L., Harris, William G., Chiodini, Robert, Nelson, Richard A, Huang, PiTien, Kruhm, and David A., "Emerging Communication Technologies Phase 2 Report," NASA/TM-2004-211522, vol. 3, September 2003.
7. Couch, Leon W. II, Digital and Analog Communication Systems, Second Edition, Macmillan, Inc., 1987.
8. Ziemer and Tranter, Principal of Communication, Fifth Edition, John Wiley and Son, 2002.
9. Aiello, G. Roberto and Roberson, Gerald D., "Ultra-Wideband Wireless Systems," Proceedings of the IEEE microwave magazine, June 2003.
10. Win, Moe Z., Scholtz, Robert A, "Impulse Radio: How It Works," Proceedings of the IEEE, vol.2 (1998): 36-38.

11. Retrieved July 28, 2004 from,
http://www.fcc.gov/Bureaus/Engineering_Technology/Orders/2002/fcc02048.pdf.
12. Ramirez-Mireles, Fernando, Scholtz, Robert, "System Performance Analysis of Impulse Radio Modulation", Proceedings of IEEE, RAWCON Conference, August (1998), pgs: 67-70.
13. Retrieved August 2, 2004 from,
http://www.intel.com/technology/ultrawideband/downloads/Ultra-Wideband_Technology.pdf.
14. Retrieved June 2, 2004 from,
http://www.win.tue.nl/~hmei/Personal/MSc_thesis_HailiangMei.pdf
15. Van Nee, Richard and Prasad, Ramjee, OFDM for Wireless Multimedia Communications, Artech House Publisher, 2000.
16. Bingham, John A. C., "Multicarrier Modulation for Data Transmission: An Idea Whose Time Has Come," Proceedings of the IEEE, vol.28 (1990): 5-14.
17. Chandler, David, "Phase Jitter Phase noise and Voltage Controlled Crystal Oscillators," Corning Corporations retrieved from,
http://www.corningfrequency.com/library/phase_jitter_note.pdf.
18. Simon, Marvin K, "A Simple Evaluation of DPSK Error Probability Performance in the Presence of Bit Timing Error," Proceedings of the IEEE, vol. 42 (1994) 263-267.
19. Lo, C.M. and Lam, W. H., "Error Probability of Binary Phase Shift Keying in Nakagami-m Fading Channel with Phase Noise," Proceedings of the IEEE, vol. 36 (2002) 1773-1774.

20. Piechocki, R.J., Kasparis, C., Nix, A. R., Fletcher P. N., and McGeehan, J. P., "Bootstrap Frequency Equalization for MIMO Wireless Systems," Proceedings of IEEE, vol.7 (2003) 4175-4179.
21. Lee, T., and Donnelly, K., "A 2.5V CMOS Delay Locked Loop for an 18 MBIT 500 Megabyte DRAM," Proceedings of IEEE, vol. 29 (1994) 1491-1496.
22. Retrieved July 15 from,
http://www.wirelessapplications.com/wireless/services/lostFound/images/Eb_No_and_S_N_Final.pdf
23. Retrieved August 15, 2004 from, <http://jove.prohosting.com/~skripty/>